U.S. DEPARTMENT OF ENERGY

PNNL-21692

Prepared for the U.S. Department of Energy
under Contract DE-AC05-76RL01830

# Nondestructive Examination (NDE) Detection and Characterization of Degradation Precursors

## Technical Progress Report for FY 2012

P Ramuhalli
RM Meyer
JM Fricke
MS Prowant
JB Coble
JW Griffin
SG Pitman
ME Dahl
TA Kafentzis
TJ Roosendaal

September 2012

Pacific Northwest
NATIONAL LABORATORY

*Proudly Operated by Battelle Since 1965*

PACIFIC NORTHWEST NATIONAL LABORATORY
*operated by*
BATTELLE
*for the*
UNITED STATES DEPARTMENT OF ENERGY
*under Contract DE-AC05-76RL01830*

PNNL-21692

# Nondestructive Examination (NDE) Detection and Characterization of Degradation Precursors

## Technical Progress Report for FY 2012

P Ramuhalli
RM Meyer
JM Fricke
MS Prowant
JB Coble
JW Griffin
SG Pitman
ME Dahl
TA Kafentzis
TJ Roosendaal

September 2012

Prepared for
the U.S. Department of Energy
under Contract DE-AC05-76RL01830

Pacific Northwest National Laboratory
Richland, Washington 99352

# Summary

The overall objective of this project was to investigate the effectiveness of nondestructive examination (NDE) technology in detecting material degradation precursors by initiating and growing cracks in selected materials and using NDE methods to measure crack precursors prior to the onset of cracking. Nuclear reactor components are subject to stresses over time that are not precisely known and that make the life expectancy of components difficult to determine. To prevent future issues with the operation of these plants because of unforeseen failure of components, NDE technology is needed that can be used to identify and quantify precursors to macroscopic degradation of materials. Some of the NDE methods being researched as possible solutions to the precursor detection problem are magnetic Barkhausen noise, nonlinear ultrasonics, acoustic emission, eddy current measurements, and guided wave technology. In FY12, the objective was to complete preliminary assessment of advanced NDE techniques for sensitivity to degradation precursors, using prototypical degradation mechanisms in laboratory-scale measurements. This present document reports on the deliverable that meets the following milestone: M3LW-12OR0402143 – Report detailing an initial demonstration on samples from the crack-initiation tests will be provided (demonstrating acceleration of the work).

# Acronyms and Abbreviations

| | |
|---|---|
| ABN | acoustic Barkhausen noise |
| AE | acoustic emission |
| AMP | aging management program |
| ASME | American Society for Mechanical Engineers |
| ASNT | American Society of Nondestructive Testing |
| BPV | Boiler & Pressure Vessel |
| BWRVIP | Boiling Water Reactor Owners Group's Vessel and Internals Project |
| CFR | Code of Federal Regulations |
| COD | crack opening displacement |
| DFEM | dynamic finite element method |
| DI | damage index |
| DOE | U.S. Department of Energy |
| EBSD | electron backscatter diffraction |
| EFIT | elastodynamic finite element integration technique |
| fc | centroid frequency |
| fcc | face centered cubic |
| GALL | Generic Aging Lessons Learned |
| IGSCC | intergranular stress corrosion cracking |
| ISI | in-service inspection |
| LTO | long-term operations |
| LWR | light-water reactor |
| LWRS | Light Water Reactor Sustainability |
| MAE | modal acoustic emission |
| MBN | magnetic Barkhausen noise |
| MRP | Materials Reliability Program |
| NDE | nondestructive evaluation |
| NLU | nonlinear ultrasonics |
| NPP | nuclear power plant |
| R&D | research and development |
| SCC | stress corrosion cracking |
| SH | shear-horizontal |
| SS | stainless steel |
| SSC | systems, structure, and component |
| TGSCC | transgranular stress corrosion cracking |

# Contents

# Figures

# Tables

# 1.0 Introduction

The U.S. Department of Energy's (DOE) Light Water Reactor Sustainability (LWRS) Program is developing the fundamental scientific basis to understand, predict, and measure changes in materials and systems, structure, and components (SSCs) as they age in environments associated with long-term operations (LTO) of operating commercial nuclear power reactors. The push towards safe long-term operations of light-water reactor (LWR) nuclear power plants (NPPs) brings significant challenges because aging of components can limit the operating lifetime of critical systems (Bond 2010; Bond et al. 2011a). A key element of LTO of LWRs is therefore expected to be the management of aging and degradation in materials that make up the passive safety system components. If not managed, degradation and aging have the potential to reduce the safety margin of nuclear components.

Within the LWRS Program, the Materials Aging and Degradation research and development (R&D) pathway conducts R&D to develop the scientific basis for understanding and predicting long-term environmental degradation behavior of materials in NPPs. These R&D products will be used to define operational limits and aging mitigation approaches for materials in NPP SSCs that are subject to long-term operating conditions. In parallel, the pathway is developing technologies for the assessment of the condition of these materials in a nondestructive fashion, as such assessments will be necessary to assure adequate safety margins and ensure that an effective aging management program can be set up for LTO.

One class of passive components of concern for LTO are metallic Class 1 components (pressure vessel, primary piping, etc.), because these systems and structures are not easily or economically upgraded when degradation is detected (Bond et al. 2008). Current approaches to detecting material degradation in LWRs use nondestructive in-service inspection methods (such as ultrasonic and eddy current inspection) periodically, typically during refueling outages. These techniques have been shown to be reliable for detecting large cracks or significant areas of corrosion in materials currently used in NPP construction. However, approaches to mitigating the growth of large cracks are limited; and for sustainable long-term operations, the need is to detect and assess degradation before the onset of large-scale cracking. Such an approach provides sufficiently early notice of potential component failure and enables proactive actions to be taken to mitigate and control degradation growth. To meet this need, nondestructive measurement methods are needed that are sensitive to the small-scale changes in material microstructure that occur as degradation accumulates.

This project addresses these issues by developing and evaluating nondestructive methods for their sensitivity to material degradation precursors. The present report describes progress towards this objective in FY 2012.

The report is organized as follows. Section 2 discusses the measurement needs and briefly reviews the state of the art in nondestructive methods for degradation precursor detection. Section 3 briefly describes the experimental setup used for this preliminary assessment. Section 4 presents a discussion of the results to date and the implications of the results. Finally, Section 5 briefly summarizes the work to date, and describes planned follow-on research activities.

# 2.0 Nondestructive Methods for Degradation Assessment

The U.S. fleet of commercial nuclear power reactors has an average age of more than 30 years, and most of the fleet has either applied for or received an extension of the operating license from 40 years to 60 years (NRC 2011). Attention is now turning to the potential for a second round of license extensions (Chockie et al. 1991; Bond 1999; Gregor and Chockie 2006; Bond et al. 2008). One challenge to safe long-term operations is the life-limiting nature of materials aging and degradation, as the resulting degradation in the structural response of the material can limit safety margins (Bond et al. 2011b). While a subset of components (such as the steam generator) may be replaced relatively easily (although such replacement might be expensive), replacement of several of the larger components, including the reactor pressure vessel and primary piping, is likely to be economically prohibitive. Thus, management and mitigation of aging-related degradation in these critical components becomes important to maintaining safety margins.

One class of components that are of particular concern is metallic components (including Class 1 components such as the reactor pressure vessel and primary piping). In the context of long-term operations, the increased exposure to time-at-temperature, along with the effects of extended irradiation and accumulated operational stresses, is expected to result in microstructural changes in the material. As a result, issues of concern (in metallic components) with respect to long-term operation include (Griffith et al. 2012):

- stress corrosion cracking;
- helium-induced degradation and cracking in weld repairs;
- phase transformations due to irradiation;
- crack initiation, especially in nickel-based alloys; and
- embrittlement and hardening of RPV steels.

Each of these degradation types, as well as other degradation mechanisms that occur in these components, likely have different underlying mechanisms (many of which are poorly understood) that drive the accumulation of damage and initiation of cracking.

## 2.1 Current In-Service Inspection Practices

From a regulatory perspective, commercial NPPs are required to demonstrate adequate safety margins through multiple, independent, and redundant layers of protection (Diaz 2004). For the United States, industry-wide aging observations for legacy nuclear plants and guidance towards the management and mitigation of the effects of passive SSC aging are tabulated in a series of extensive reports called the Generic Aging Lessons Learned (GALL) reports (NRC 2001, 2005a, b, 2010b). These reports provide the technical basis for determining whether plant aging management programs (AMPs) at operating reactors are adequate or need modification as plants enter extended operation. The AMP applies to all SSCs that are safety-related or whose failure could affect safety-related functions, as well as those SSCs relied on for compliance with fire protection, environmental qualification, pressurized thermal shock, anticipated transients without scram, or station blackout regulations. Specific programs that need

modification are also identified, and the information in these reports are also included in the NRC's Standard Review Plan for Review of License Renewal Applications (NRC 2010a).

One component of the AMP is the scheduled in-service inspection (ISI) of passive components, codified in 10 CFR 50.55a (2007), which specify the requirements for nondestructive inspection (such as inspection periodicity, inspection techniques, and qualification procedures). These elements are contained in the American Society for Mechanical Engineers (ASME) Boiler & Pressure Vessel (BPV) Code, which the Code of Federal Regulations (CFR) incorporates by reference. The ASME Code specifies the minimum requirements for NDE. Specifically, Section XI of the Code defines the acceptable volumetric and surface examination techniques, minimum requirements for acceptable procedures, and the acceptance criteria for flaws that are detected. In addition, requirements for qualification of the procedures, equipment, and personnel are specified to ensure reliable inspections. Currently, degradation in metallic components is managed through periodic ISI as mandated by the ASME BPV Code, with risk-based principles used to determine ISI intervals and the components scheduled for inspection in any given interval. Nondestructive inspection methods that are approved by the Code are generally categorized into volumetric and surface examination techniques. Volumetric examination techniques include ultrasonic examination, radiographic examination, and eddy current examination, and are approved for flaw detection below the surface. Surface examination methods (including eddy currents, visual, magnetic particle, dye penetrant) are applicable for the detection of surface-breaking cracks.

In the United States, for certain inspection techniques and components, the nuclear industry has developed additional examination guidelines, such as those developed under the Boiling Water Reactor Owners Group's Vessel and Internals Project (BWRVIP) program, and the Materials Reliability Program (MRP) (for instance, EPRI 2008; EPRI 2011). A number of studies have also examined the reliability of NDE techniques (Chockie 1981; Doctor 1984; Fong 1986; Bates et al. 1987; Nichols and McDonald 1987; Willetts and Ammirato 1987; Doctor et al. 1995; Doctor 2007; Miller 2008) and determined that several sources of variability were present that impacted the reliability of NDE. These results were codified in Section IX, Appendix VIII of the ASME BPV Code, and are the basis for performance demonstration procedures for NDE techniques (Chockie 1985).

While the ISI program for metallic components has been in existence for a number of years, there are significant challenges associated with ISI for long-term operations, due to the combination of new (and possibly currently unknown) degradation mechanisms (Wilkowski et al. 2002) and the increase in the number of components that become susceptible to aging-related degradation as plants transition to long-term operations (Doctor 1988). Current NDE techniques for ISI are typically applied to detect large flaws that occur near the end of component life. To manage aging, license extensions for LTO [i.e., 60–80 years] will likely require a shift to a more proactive approach to aging management in addition to updated approaches to periodic ISI to ensure earlier detection of degradation and timely application of mitigation strategies (Bond et al. 2008; Hines et al. 2008; Bond 2010).

Three overarching elements of research are necessary to develop a proactive aging management philosophy and these include:

- Integration of materials science understanding of degradation accumulation, with nondestructive measurement science for early detection of materials degradation.

- Analysis methods for condition assessment that can be utilized for remaining life estimation from measurement data.
- Development of robust sensors and instrumentation, as well as deployment tools, to enable extensive condition assessment of passive NPP components.

This project addresses the first two elements using a phased approach.

## 2.2 NDE for Degradation Detection in NPPs

Degradation and aging issues in NPP have been the subject of extensive literature going back many years (Shah and MacDonald 1993; Livingston et al. 1995; Morgan and Livingston 1995; IAEA 2003; NRC 2005a, b; Andresen et al. 2007; IAEA 2007; NRC 2010b; IAEA 2011). These insights are supplemented by several expert panel review reports that tabulated data on materials and specific component susceptibility to known or expected degradation (Andresen et al. 2007; Lain 2008; Pathania 2008; Stark 2008). New degradation processes have appeared in the current LWR fleet, on average, at a rate of one new form of degradation every seven years (Wilkowski et al. 2002).

Aging and degradation mechanisms are usually classified into two main categories: (1) those that affect the internal microstructure or chemical composition of the material and thereby change its intrinsic properties (e.g., thermal aging, creep, irradiation damage), and (2) those that impose physical damage on the component either by metal loss (e.g., corrosion, wear) or by cracking or deformation (e.g., stress-corrosion cracking). Of the different degradation mechanisms prevalent in LWR materials, stress corrosion cracking in its many variants plays a major role in the potential reduction in structural integrity.

The challenges associated with characterization of aging in NPP materials, especially irradiated reactor components, are significant, requiring understanding of microstructural changes prior to crack initiation and growth. The challenges associated with characterization of aging in NPP materials, especially irradiated reactor components, are significant (Doctor 1988; Dobmann 2006). In most cases of degradation, change in the intrinsic material properties is dominant in the early stages. When the accumulation of such damage exceeds a critical limit, physically observable damage will start. There is a possibility that such early physical damage can be detected as the change of locally averaged material properties with appropriate sensors (Inman et al. 2005; Bond et al. 2008; Bond et al. 2009b).

Current NDE techniques used for NPP ISI to detect materials degradation are typically applied to detection of large flaws that occur near the end of component life. However, recent years have seen a move towards NDE for early damage detection in NPP materials (Bond et al. 2009a, 2011a). Methods for early detection of materials degradation require novel sensors and enhanced data integration techniques. A range of acoustic and electromagnetic measurement methods may be suitable for this purpose (Ramuhalli et al. 2010; Ramuhalli et al. 2011).

A survey of the technical literature (Meyer et al. 2011) has identified a number of promising NDE methods for the detection of crack precursors in metals. Additional reviews of the literature were conducted to identify the advantages and disadvantages of these methods, and to identify a set of potential methods for preliminary assessment. The methods include:

- **Ultrasonic velocity and attenuation**: These techniques use classical ultrasonic measurement methods to measure the velocity and attenuation, potentially as a function of frequency, and have been shown to be sensitive to a range of degradation mechanisms.
  - **Bulk wave** measurements use body or bulk waves to measure the velocity and attenuation, usually as a function of wave mode (longitudinal or shear).
  - **Guided wave** measurements have been proposed as a potential technique for long-range examination of components such as piping. The method uses the structure or component as a waveguide to propagate the applied stress waves over long distances. Sensitivity to large-scale cracking has been shown in prior studies.
- **Acoustic emission (AE)**: AE is a passive technique that "listens" for stress waves initiated by the onset of cracking or other dislocation movement. AE has been shown in prior work to be sensitive to crack growth (Hutton et al. 1993). A potential challenge is to discriminate crack growth signals from environmental noise.
- **Nonlinear acoustics** (Cantrell and Yost 2001; Ogi et al. 2001): This class of techniques attempts to measure the relative change in the nonlinear elastic wave response of the material due to accumulated damage. Techniques included in this method can employ:
  - Bulk measurements (Cantrell and Yost 2001)
  - Rayleigh wave measurements (Shui et al. 2008)
  - Guided wave measurements (Bermes et al. 2008)
- **Micromagnetic measurements** (Raj et al. 2003; Dobmann 2006; McCloy et al. 2012): These generally refer to magnetic Barkhausen noise (MBN) and acoustic Barkhausen noise (ABN). These signatures (signals) are a result of magnetic hysteresis in ferromagnetic materials (or materials with a ferromagnetic phase) and are a result of magnetic domain pinning by dislocations or other pinning sites.
- **Eddy currents** (Lois and Ruch 2006; Ramuhalli et al. 2010): This method relies on the change in electrical impedance of a coil due to induced currents in the material. The induced current depends on the electrical conductivity and magnetic permeability of the material, as well as the frequency of the applied electromagnetic field.

However, the sensitivity of these techniques to precursors from damage mechanisms of interest to LWR long-term operations is not clear and needs to be quantified. Further, there are still no accepted measurement technologies for the detection and assessment of some degradation mechanisms unique to NPPs, such as void swelling.

In FY 2012, this project's focus was on the preliminary assessment of advanced NDE methods—magnetic Barkhausen noise, nonlinear ultrasonics, and acoustic emission—using mechanical and thermal fatigue as prototypic damage mechanisms, to evaluate sensitivity to precursors and optimize system setup prior to beginning extensive evaluations on detection sensitivity for SCC precursors in FY2013. In this, both the thermal fatigue setup from the previous year, as well as a mechanical fatigue setup available in the laboratory, was used for measurement system optimization. Measurement methods that were evaluated during the current phase of the project are described below.

## 2.3 Magnetic Barkhausen Noise

The magnetic Barkhausen effect is a result of the magnetic hysteresis of ferromagnetic materials (Jiles 2000; Stupakov et al. 2008). The magnetic flux density in ferromagnetic materials placed in an external applied magnetic field is a function of the applied magnetic field, with larger numbers of magnetic domains within the material aligning with the applied field direction with increasing applied field strength. This realignment is, however, not a continuous process, because the presence of dislocations or other damage precursors results in domain wall pinning. Increasing the applied field strength results in abrupt realignment of some domains, and is accompanied by a release of energy that may be detected using a sensing coil (Figure 2.1). Studies indicate that the magnetic Barkhausen effect in many materials is primarily due to the motion of 180° domains, and its interactions with dislocation tangles (Ranjan et al. 1987a; Krause et al. 1994). The number of Barkhausen counts is given by Ranjan et al. (1987b)

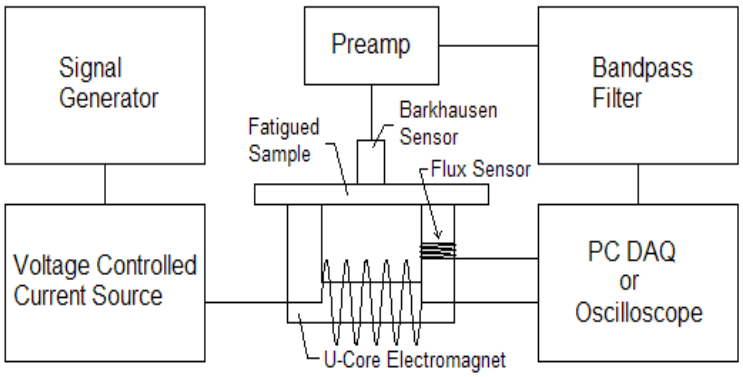


**Figure 2.1**. Schematic of MBN Measurement System

$$N_{MB} = c' \int \rho_{180}(H) \bar{V}_{180}(H) \overline{\overline{\Delta B}} dH \tag{2.1}$$

where $c'$ is a constant that depends on the time constant of the pickup coil, permeability, and conductivity of the sample; $\rho_{180}(H)$ is the density of 180° domain walls at field $H$; $\bar{V}_{180}(H)$ is the average critical velocity of a 180° domain wall when it is released from pinning sites; and $\overline{\overline{\Delta B}}$ is the average change in the local magnetic induction due to unit displacement per unit area of domain walls. Note that two Barkhausen bursts are present—one for the positive magnetization and the other for negative magnetization. Numerous models have been developed to predict Barkhausen response to microstructural defects in steels such as grain boundaries and second phase precipitates (Kameda and Ranjan 1987; Moorthy et al. 1997; Perez-Benitez et al. 2005).

Like all electromagnetic methods, the magnetic Barkhausen method is predominantly a near-surface measurement, with the standard depth of penetration (the distance into the material where the induced current density decreases to 37% of its value at the surface) decreasing with increasing frequency (ASNT 2004) defined as:

$$\delta = \sqrt{\frac{1}{\pi f \mu \sigma}} \tag{2.2}$$

where $f$ is the excitation frequency, $\mu$ is the magnetic permeability of the material, and $\sigma$ is the electrical conductivity. For non-ferritic steel (such as 304 or 316L), the skin depth at 1 kHz is about 13.1 mm.

In many stainless steels, the effect of increasing damage (through mechanisms such as fatigue loading) is an increase in dislocation density. At the same time, in certain steels, damage can result in conversion of austenite to a ferritic phase. The impact of these changes is two-fold, resulting in local changes in conductivity and permeability. These phenomena combine to impact the Barkhausen noise measurement from steels subjected to aging and degradation. However, the correlation between the measured parameters and the amount of damage is not linear, and is a function of several other variables (such as hardness). The Barkhausen noise measurement method has been applied to determine residual stresses in ferritic steels, and to determine the amount of hardening or cold work. Studies have also shown that this technique is sensitive to damage precursors in ferromagnetic materials, and quantities such as the energy and peak value in the Barkhausen signal have been shown to correlate well with level of damage in materials (Parakka et al. 1997; Gorkunov et al. 2000; Sullivan et al. 2004; Sagar et al. 2005; Hakan Gur and Cam 2007).

While a number of studies have linked degradation accumulation to magnetic Barkhausen noise, there are still many sources of uncertainty when using this nondestructive measurement method. Fundamentally, a great deal of uncertainty is introduced by the fact that damage accumulation and crack initiation is a stochastic process (Sobczyk and Kirkner 2001). Thus, the location where the MBN measurement is made is likely to introduce some uncertainty. Further, the measurement process (i.e., manual or automated probe placement, probe coupling pressure, etc.) also adds some error. These sources of error apply to other measurement methods as well. In addition, the MBN measurement is subject to uncertainty due to:

- Orientation of the tensile strain direction, relative to the applied external field direction and the magnetic easy axis (Krause et al. 1995);
- Specimen fabrication variability as well as residual stress in the specimen (Krause et al. 1995; Lindgren and Lepistö 2001);
- Number, location, and orientation of magnetic domains. In particular, in two-phase steels, the volume fraction and distribution of the ferromagnetic phase will have a significant impact on the recorded measurement (Csikor et al. 2007).

The measurement protocol in this study is selected to address some of these sources of uncertainty.

## 2.4 Acoustic Emission

A detailed history and introduction to acoustic emission testing is provided in the American Society of Nondestructive Testing (ASNT) Handbook (ASNT 2005). Fundamentally, acoustic emission is the elastic energy released during deformation of materials (ASNT 2005). The released energy travels as a transient elastic wave in the material and is typically recorded using a transducer that is located at some distance from the AE source. In metals, several phenomena give rise to AE, including crack initiation and

growth, phase transformations, twinning, deformation, etc. Factors such as leaks also give rise to changes in the local stress gradients, resulting in a transient elastic wave.

For metals experiencing mechanical degradation, several phenomena can be responsible for the generation of AE. These phenomena include ((Sinclair et al. 1977; Berkovits and Fang 1995; Mukhopadhyay et al. 1998; Shaira et al. 2008) dislocation generation and motion, martensite formation, twinning, fracture and decohesion of inclusions and precipitates, plastic deformation, crack propagation, and crack closure/rubbing. Several of the above phenomena exhibit distinct behaviors with respect to time. AE from crack propagation and decohesion of inclusions and precipitates are discontinuous and occur as discrete "bursts" of energy (Harris and Dunegan 1974), while dislocation motion and generation processes result in the continuous release of energy (Mukhopadhyay et al. 1998; Mukhopadhyay et al. 2000). Many source events may be treated as point discontinuity in which the AE energy is emitted symmetrically in all directions assuming the material is uniform and isotropic. As the AE signal propagates through a test component, the signal will experience attenuation due to the effects of geometric spreading in addition to any material absorption. In thick components, theory of bulk ultrasonic wave propagation may be applied to model the propagation of AE signals while in thinner components, propagation of AE signals may be treated by the theory of guided ultrasonic waves. Basic theory behind the propagation of guided ultrasonic waves in planar components can be found in many texts including the text by Rose (1999). In planar components, low-frequency ultrasonic energy is propagated as Lamb waves. Lamb waves can consist of an infinite number of symmetric, $S_n$ (n = 0,1,2,…), and anti-symmetric, $A_n$ (n = 0,1,2,…), modes. Dispersion relationships for the group velocity, Vg, and phase velocity, Vp, of Lamb waves in a 10-mm-thick steel plate are shown in

Figure 2.2. This figure shows that only the fundamental Lamb wave modes, A0 and S0, are supported at low frequencies.

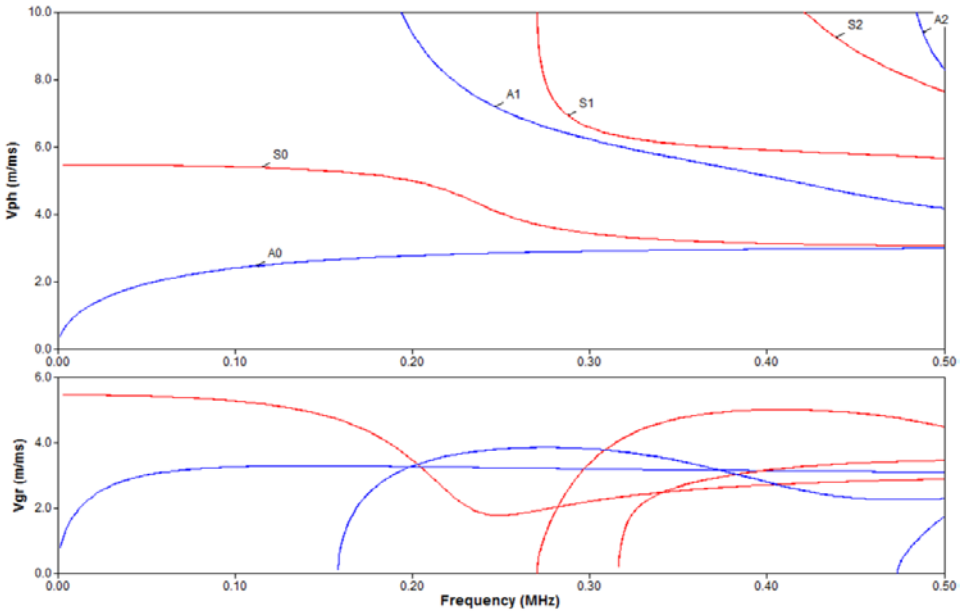


**Figure 2.2**. Dispersion Relationships for the Group Velocity, Vg, and for the Phase Velocity, Vp, of Lamb Waves Excited in a 10-mm-thick Steel Component

Guided waves polarized perpendicular to Lamb waves and with the wave displacement perpendicular to the surface normal and direction of propagation are referred to as shear-horizontal (SH) waves. At low enough frequencies, only the fundamental mode (SH0), is supported and propagates at the velocity of bulk shear horizontal waves (3.26 m/ms in steel).

Modal acoustic emission (MAE) is used to refer to the techniques of analysis of the wave propagation of AE signals. In the limit that component thickness goes to zero or is very small, the full Lamb wave solutions reduce to the plate wave solutions. Plate wave theory predicts the propagation of two modes: an extensional (S0 – displacement in-plane) mode and a flexural (A0 – displacement out of plane) mode. In addition to these modes, investigators have reported the propagation of a significant shear mode (displacement in-plane and perpendicular to the direction of propagation) (Dunegan 1997; Surgeon and Wevers 1999). The extensional and shear modes are dispersionless (constant with frequency) while the flexural mode velocity scales with the square root of frequency. Gorman and Prosser (1991) report that AE sensors mounted to the surface of a plate should be most sensitive to flexural mode signals because they have their greatest displacement out-of-plane of the plate. Dunegan (1997) postulates that shear modes are the most likely modes sensed on large field structures because they are consistently found to have greater amplitudes than extensional mode signals and do not undergo mode conversions upon reflections. MAE has been explored as a technique to discriminate between various source mechanisms. Both pencil lead breaks (Gorman 1991) and real damage have been shown to generate plate modes (Gorman and Ziola 1991). Gorman (1991) explored the impact of source orientation through pencil lead breaks at several angles in aluminum and graphite/epoxy plates and found that the relative amplitudes of the flexural and extensional modes were dependent on the source orientation. Further, the relative amplitudes of extensional and flexural mode signals were dependent on whether sensors were mounted on the surface or the edge of plates. Dunegan (1997) reports that shear waves will be sensitive to both out-of-plane noise sources and in-plane signals from crack growth and are therefore not sufficient for distinguishing between the two. Flexural modes are described as the most effective for identifying noise so the deployment of sensors sensitive to both the flexural mode and shear mode are recommended for distinguishing the source of the signal based on the relative amplitudes of the flexural and shear components. Gorman and Ziola (1991) noted that most location algorithms for AE signals assume that they propagate at a single velocity and explored the impact of simultaneous multi-mode propagation on locating AE signals. Surgeon and Wevers (1999) consider a technique for AE source location that takes advantage of the modal behavior of AE signal propagation to reduce the number of sensors needed for location. Essentially, the technique is based on measuring the relative arrival times of extensional and flexural modes and their known velocities to determine the location of a source using a single sensor.

Theoretical studies of the propagation of AE signals through materials have followed experimental efforts related to MAE. Schubert and Schechinger (2002) discuss the use of the elastodynamic finite element integration technique (EFIT) to model AE wave propagation for application to monitoring of concretes structures. The implementation of various source discontinuities such as tension cracks, shear cracks, and volume expansion is demonstrated. Prosser et al. (1999) apply the normal mode solution method for Mindlin plate theory to predict the response of the flexural plate mode to a point source, step-function load, applied on a plate surface. Dynamic finite element method (DFEM) is used to model the problem from equations of motion based on exact linear elasticity. Calculations made for both isotropic and anisotropic cases of DFEM is described as having greater flexibility in modeling complex different source configurations and geometries. The Mindlin plate theory would not be useful for modeling in-

plane sources such as fatigue cracking or matrix cracking, which generate large extensional mode signals with little or no flexural modes.

Generally, the mechanisms responsible for AE during corrosion are not characterized as well as mechanisms responsible for AE from mechanical damage (Lenain and Proust 2005). Some of the corrosion processes that could result in AE are film cracking, gas evolution, hydrogen migration, plastic zone formation, stress corrosion cracking (SCC), and hydrogen cracking (Shaikh et al. 2007). The evolution of hydrogen gas by cathodic reactions and the breakdown of thick surface oxide films have also been identified as suspected sources of AE during SCC and corrosion processes by Yuyama et al. (1984). In addition, it is noted that several phenomena can contribute to total detectable AE during crack extension, including the following (Yuyama et al. 1984): martensitic transformation, slip deformation, twinning, fracture and decohesion of precipitates, second-phase particles, or non-metallic inclusions, and microcracking.

Corrosion processes accompanying SCC can mask the AE signals produced by cracking (Yuyama et al. 1984; Jones and Freisel 1992) unless signals produced by corrosion processes can be distinguished from SCC. Discrimination between AE activity from corrosion processes and cracking is often based on amplitude as cracking signals are more energetic than signals released by corrosion processes (Ramadan et al. 2008). It has been observed in the laboratory that transgranular stress corrosion cracking (TGSCC) and intergranular stress corrosion cracking (IGSCC) processes can result in different levels of AE activity. AE monitoring of SCC in face centered cubic (fcc) materials has shown that TGSCC is an order of magnitude more active than IGSCC in terms of AE (Alvarez et al. 2008). In several studies, AE activity has been recorded before, during, and after SCC initiation (Sung et al. 1997; Shaikh et al. 2007; Ramadan et al. 2008; Du et al. 2011). It has been observed that AE is sensitive to localized corrosion phenomena that precede SCC initiation, implying the utility of AE as a precursor monitoring tool for SCC through the detection of preceding localized corrosion. Some controversy surrounds the source of AE signals during localized corrosion, but signals are generally attributed to hydrogen bubble break-up, oxide film cracking, or dislocation motion and plastic deformation (Shaikh et al. 2007).

## 2.5 Nonlinear Ultrasonics

In recent years, nonlinear ultrasonics (NLU) has seen increased interest as a means of characterizing the internal damage state of the material early in the fatigue process (Cantrell and Yost 2001; Matlack et al. 2012b). Conventional ultrasonic methods, currently in use in ISI, apply high-frequency (in excess of 500 kHz, typically around 2.25 MHz) acoustic energy and measure the resulting response due to scattering and reflection of the energy at interfaces. The presence of cracking is detected by means of a reflection from the crack surface. Other forms of damage may be detected by making use of velocity and attenuation measurements through one or more measurement configurations. However, most such measurements are not sensitive to earlier stages of damage. In contrast, NLU methods rely on the generation of harmonics from an initially monochromatic input. The generation of harmonics is due to nonlinearities in the elastic constants associated with the material (Zarembo and Krasil'nikov 1971). The second harmonic is of particular interest, and the resulting nonlinear material parameter is represented by $\beta$ (Kyung-Young 2000). A schematic of a typical single-sided measurement setup for nonlinear acoustics measurements is shown in Figure 2.3. Alternative setups that use a transmitting probe to transmit acoustic energy through the specimen and a receiving probe on the opposite side of the specimen (through-transmission mode) are also possible, as are methods that generate surface waves.

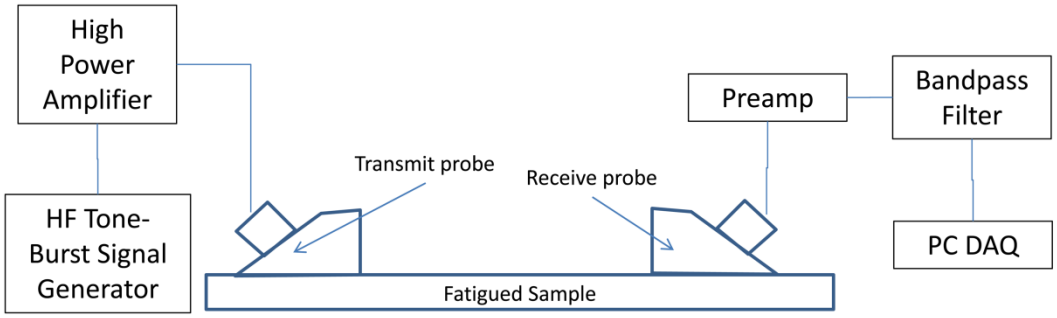


**Figure 2.3**. Schematic of NLU Measurement System

NLU has been applied to the characterization of a range of damage mechanisms, including fatigue (Kyung-Young 2000; Cantrell and Yost 2001), irradiation embrittlement (Matlack et al. 2012b), SCC (Shintaku et al. 2010; Matlack et al. 2012a), and corrosion pitting (De et al. 2010).

# 3.0 Experimental Methods

A series of experiments were carried out in the laboratory, using tensile strain and thermal fatigue as the prototypical damage mechanisms, to assess the various NDE methods for materials aging monitoring and precursor detection. The objective of these scoping studies was to evaluate variables that can impact measurement accuracy and repeatability, and evaluate approaches to improving accuracy and repeatability prior to assessing sensitivity for stress corrosion cracking.

For tensile measurements, ASTM-standard tensile specimens were fabricated using both 304 and 410 grades of steel, with a gauge length of 152.4 mm and specimen thickness of 9.5 mm. The specimens were annealed prior to the tensile test to ensure that all samples had the same initial stress state. Each specimen was held in an Instron MTS machine and uniaxial tensile stress applied, to reach uniaxial tensile strain increments of approximately 2%. During the application of strain, acoustic emission measurements were taken using two transducers spaced 140 mm apart (Figure 3.1). A linear location algorithm was selected with AEWin software in an attempt to locate the position of AE signal sources. Pencil lead break tests are performed after the initial installment of AE sensors on the tensile specimen. Breaks are performed at five locations (10 breaks at each location): the center of the specimen, near sensor 1 (bottom of specimen), near sensor 2 (top of specimen), near bolt attachment 1 (contact with load frame – bottom), and bolt attachment 2 (contact with load frame – top). After each cycle of stress application, the stress was released, the AE sensors removed, and other nondestructive measurements made on the specimen. This process was repeated until the specimen failed.

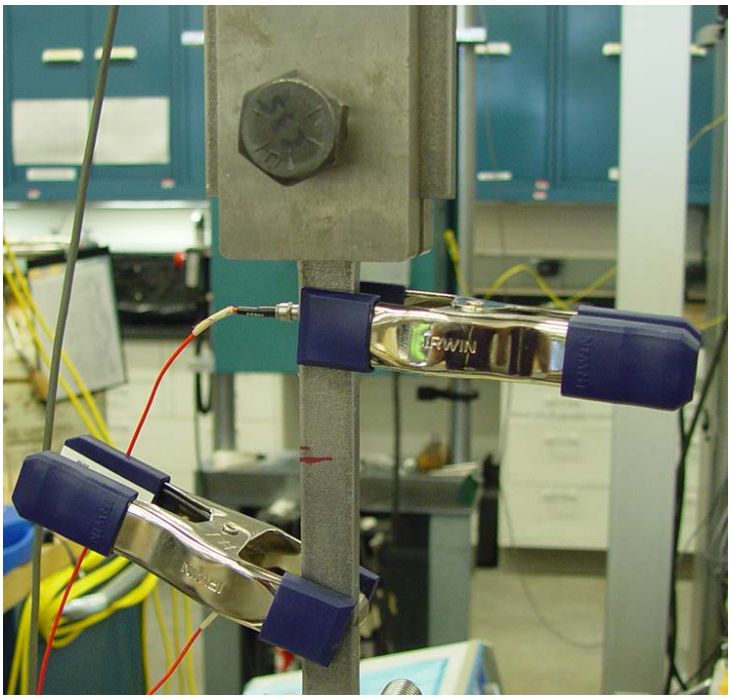


**Figure 3.1**. Photograph of AE Sensors Clamped to Tensile Specimens During Tensile Strain Tests

Magnetic Barkhausen measurements were made at three locations (top, center and bottom, labeled A, B and C) (Figure 3.2) using a Stresstech Model 300 Rollscan Barkhausen analyzer (Figure 3.3), with a Barkhausen pickup sensor (Figure 3.4). Locations A and C were approximately 76.2 mm apart and symmetric about the center of the specimen. At each location, the measurements were made with the applied magnetization direction parallel and perpendicular to the applied strain direction. The expectation was that the measured data at these locations would be similar (within measurement noise) until such time as damage localization occurred, at which point the three sets of measurements should start to deviate. For each location and magnetization direction, three measurements were made to assess repeatability and quantify measurement noise levels. Probe placement was done manually, with the probe lifted away from the surface between successive measurements.

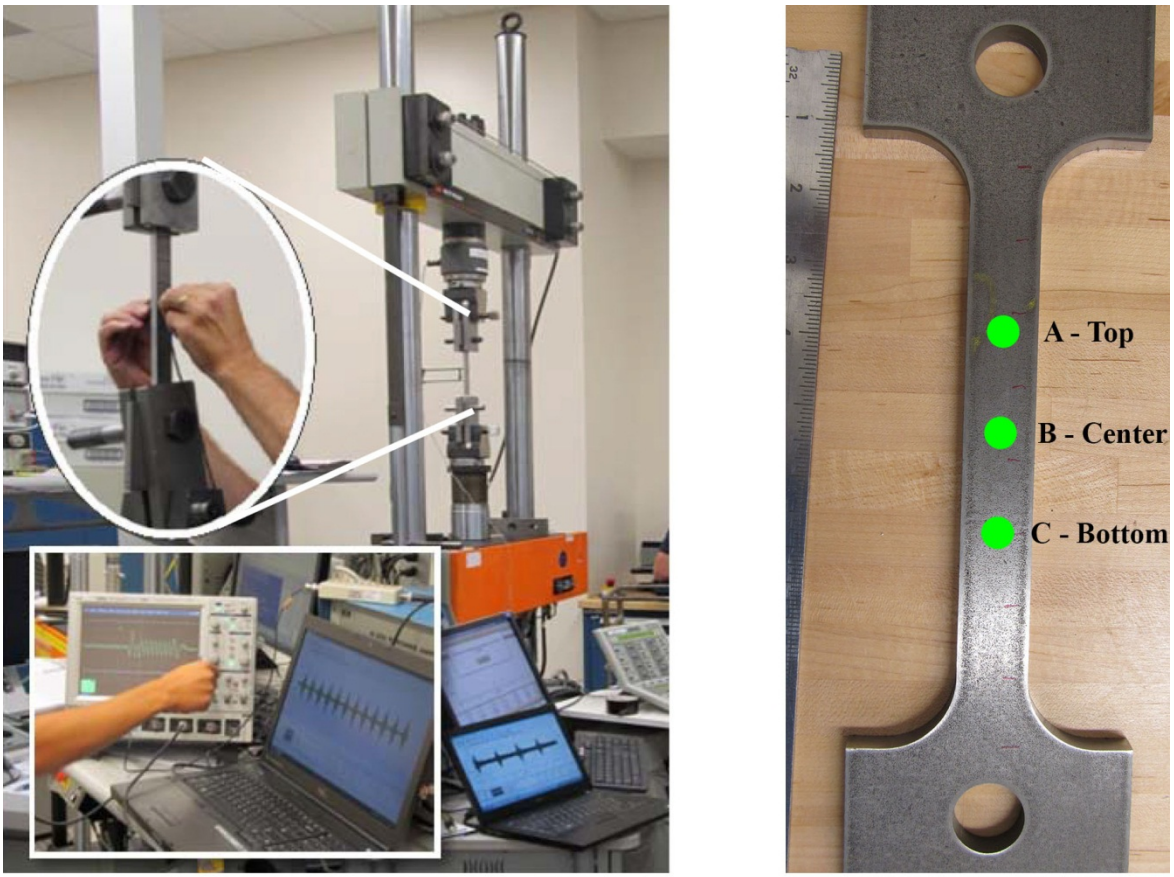


**Figure 3.2**. (a) Experimental Setup for Tensile Test; (b) Measurement Locations on Tensile Specimen

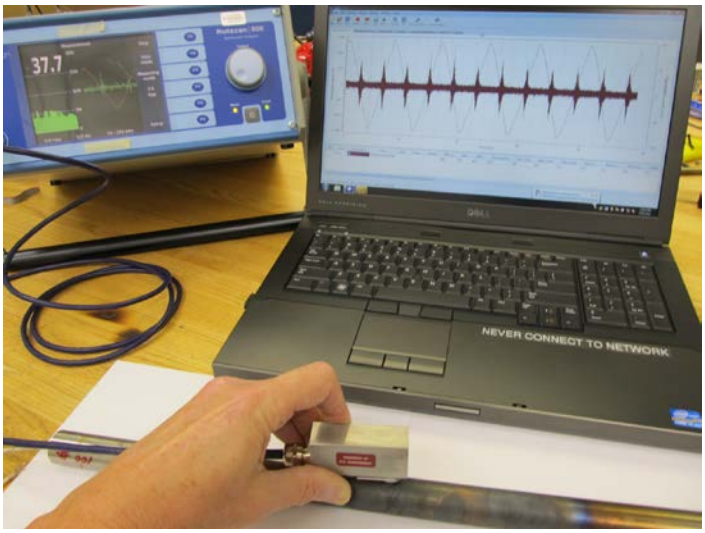


**Figure 3.3**. Stresstech Model 300 Rollscan with Microscan 600 Controller Software

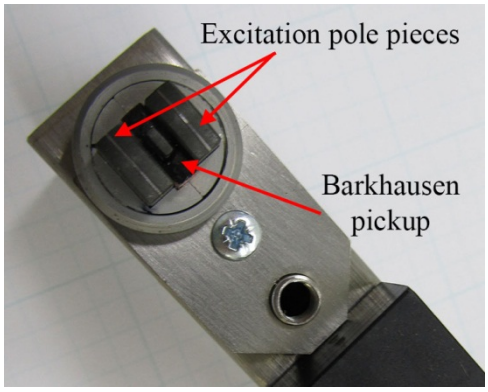


**Figure 3.4**. Detail of MBN Sensor Showing the Excitation Magnet and Pickup Sensor

NLU measurements were made on these specimens using two arrangements. In the first (through-transmission mode), the transmit and receive probes were on opposite faces of the specimen and aligned center-to-center. This pitch-catch arrangement was placed at the center of the specimen. The transmit probe had a center frequency of 5 MHz with a bandwidth of approximately 60%. The receiving transducer had a center frequency of 10 MHz with approximately the same bandwidth. Various coupling mechanisms were evaluated in the laboratory, including glue, gel couplant, and dry couplant membranes before the gel couplant was selected as the couplant of choice. A 5-cycle tone burst signal at an incident frequency of 4.5 MHz was applied to a power amplifier (ENI A-300). The output of the power amplifier was transmitted using the transmit transducer, and the resulting response was recorded using the receiving transducer, connected to a LeCroy 64xi digital oscilloscope. The data was digitized at 500 MHz prior to saving to disk. This process was repeated using tone bursts at 5 MHz and 5.5 MHz. At each frequency, three different input power levels (corresponding to an input voltage to the power amplifier of 100 mV, 200 mV, and 300 mV) were applied to the ultrasonic probe. Probe coupling force was controlled by using

a mechanical fixture to hold the transmitting and receiving probes in contact with the specimen. In this arrangement, the nonlinear parameter that is computed is based on the longitudinal wave mode.

The second approach to recording NLU measurements was using a guided wave approach. The transmitting and receiving transducers were mounted on Rexolite wedges, which enabled an incident angle in steel of 45°. The wedges were separated so that the acoustic path length in the specimen was 103 mm ±0.1 mm (the total path length in Rexolite was 41.4 mm). The tone burst, frequencies of operation, and input power levels were all the same as that for the through-transmission arrangement above. In this arrangement, the nonlinear parameter that is computed requires a dispersion analysis to identify the different modes and their propagation velocities.

As indicated earlier, thermal fatigue was chosen as the other degradation mechanism in the initial phase of this project. Tubular specimens (Figure 3.5) were selected to obtain a bench-scale thermal fatigue setup that also enabled relatively easy online nondestructive monitoring. The tubular specimens were heated from the inside with periodic cooling on the outside. Heating was accomplished by means of a cartridge heater on the inside of the hollow specimen (Figure 3.5), while cooling using the water spray was from the outside. The resulting thermal stresses initiate a crack (thermal fatigue crack) on the outside surface of the hollow specimen, providing easy access for both online (either continuously or in interrupted test mode) and offline (i.e., by removing the specimen from the test setup) NDE measurements as well as planned destructive analysis of the specimens.

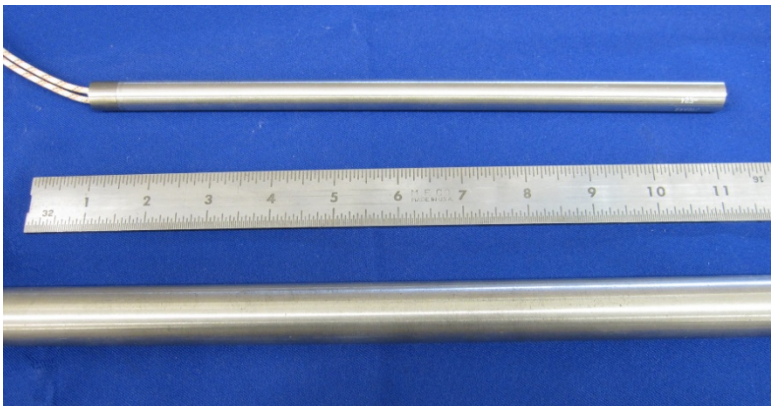


**Figure 3.5**. Example of Tubular 304SS Specimen and Cartridge Heater

Two test stations with hollow 304 stainless steel (SS) rods were designed and fabricated for this study (Figure 3.6). At each station, one specimen was heated to temperatures up to 600°C and cooled to temperatures as low as 30°C by a periodic water spray controlled by a timed solenoid valve arrangement. Figure 3.7 presents a snapshot of the fatigue process in operation at both stations, with one specimen (upper) just starting the heating cycle while the other (at the bottom of the figure) just starting the cooling cycle. Thermocouples were used to monitor and control the heating and cooling cycles. A portion of the cyclic thermal data is shown in Figure 3.8 for one of the tests that produced a thermal fatigue crack. The thermal cycles for these runs were set to be 4–5 seconds of water cooling and a total cycle length of 50 seconds, or 72 cycles per hour. This amount of cooling allowed the sample temperature to drop from

about 600°C to 30°C in the center portion of the heated rod for a maximum thermal fatigue stress. These settings caused a thermal fatigue crack, shown in Figure 3.9, to form after approximately 10,000 cycles.

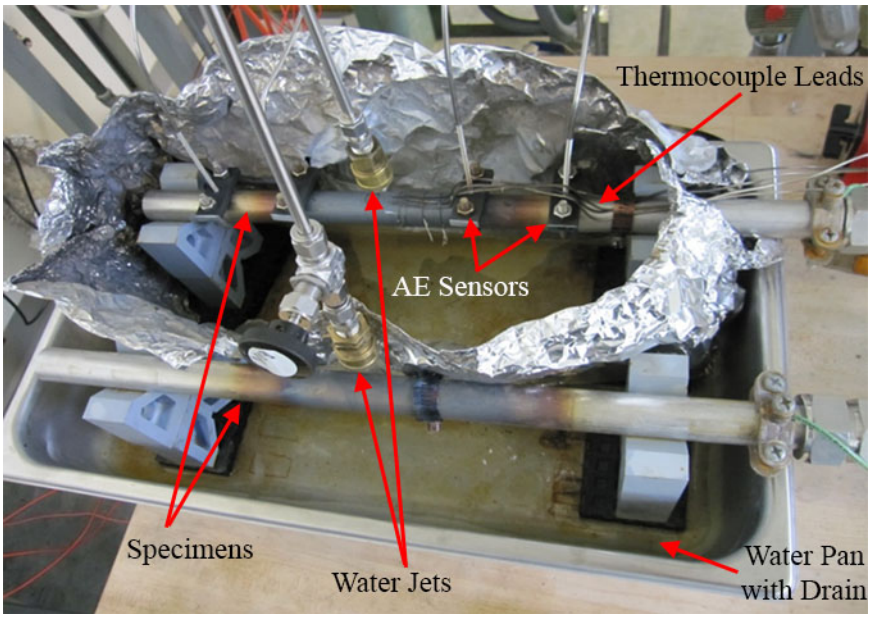


**Figure 3.6**. Thermal Fatigue Setup with Two Stations. Tubes are heated and cooled independently at each station. The setup shown has a water pan with drain, two water jets that impinge on the top of the heated specimens, assorted control and recording thermocouples, and acoustic emission sensors attached with clamps to the upper sample.

**Figure 3.7**. Thermal Fatigue Setup Operation. The upper sample has cooled below the visible thermal temperature while the lower sample has just started the cooling cycle and is still red hot. The shape of the water jets can be seen in this photo, most clearly for the upper sample.

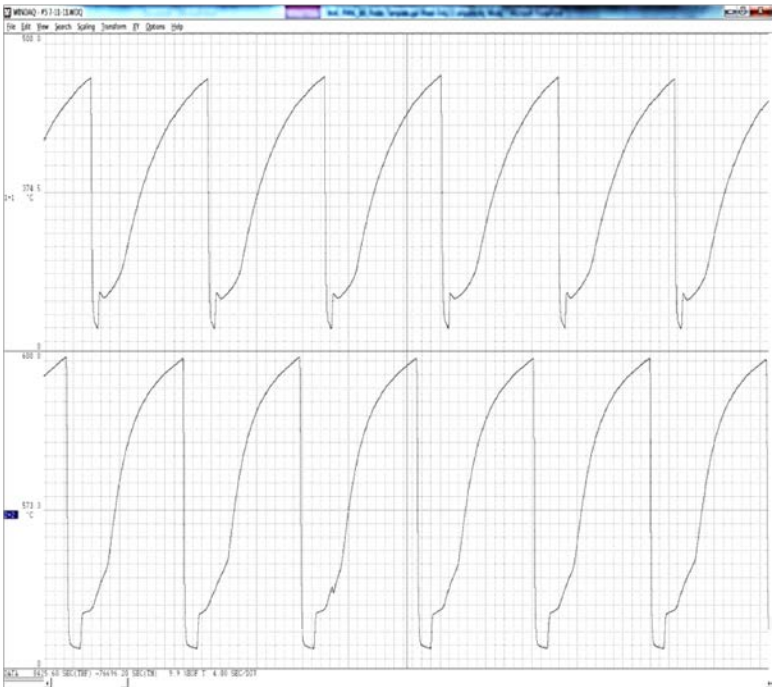

**Figure 3.8**. Sample of the Temperature Variation for Both Operating Stations Showing the Heating-Cooling Cycles that Develop Due to Constant Heating and Intermittent Water Jet Cooling

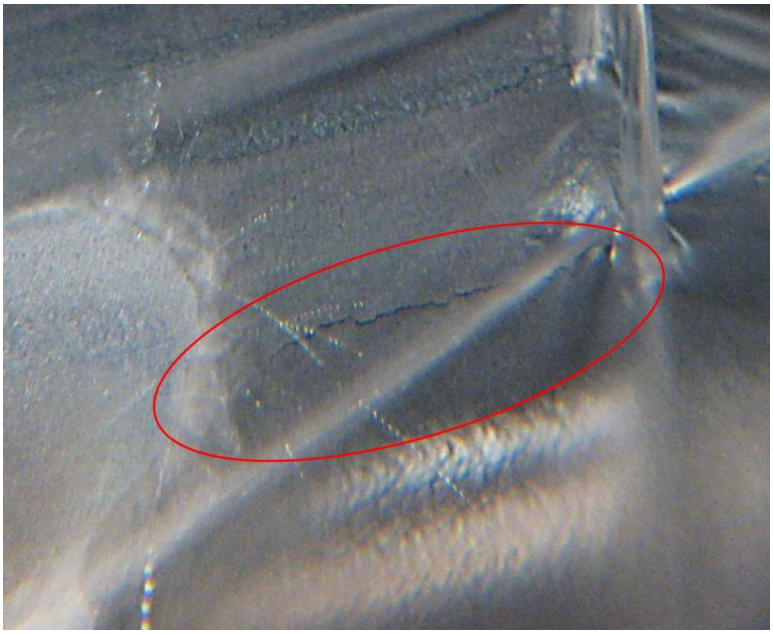

**Figure 3.9**. Thermal Fatigue Crack in a Specimen. The crack is generally visible only during the cooling portion of the fatigue cycle. At other times, high residual compressive stresses tend to exist, resulting in a small crack opening displacement (COD) that makes the crack difficult to visualize. The red oval is circling the thermal fatigue crack.

Acoustic emission was employed to perform preliminary proof-of-concept monitoring of thermal fatigue damage induced in the specimens. The thermal fatigue specimens were instrumented with a linear array of acoustic emission transducers (Figure 3.6) each coupled to the specimen through waveguides to protect and isolate the transducers from the temperature at the surface of the specimen. Four R15α transducers (Physical Acoustics Corporation) with resonant frequencies near 200 kHz were attached along the length of the specimen. The waveguides consisted of 24-in.-long cylindrical stainless steel rods with a diameter of 0.125 in. Figure 3.10 presents several different views of the setup, showing details of the AE sensors and attachment of waveguides along the length of the specimen. An eight-channel digital acoustic emission system, model MicroDISP (Physical Acoustics Corporation), was employed to record and process acoustic emission signals. Interfacing with the system was conducted through the AEWin software (Physical Acoustics Corporation) located on a laptop computer. The MicroDISP acoustic emission processor allows for input of external parametric signals. Temperature cycles were recorded by the acoustic emission system to assist in data analysis. A sample plot of recorded temperature cycles is included in Figure 3.11. Pencil lead break tests were also conducted as a quick functional check and as a means to verify the location accuracy of the AE sensor array.

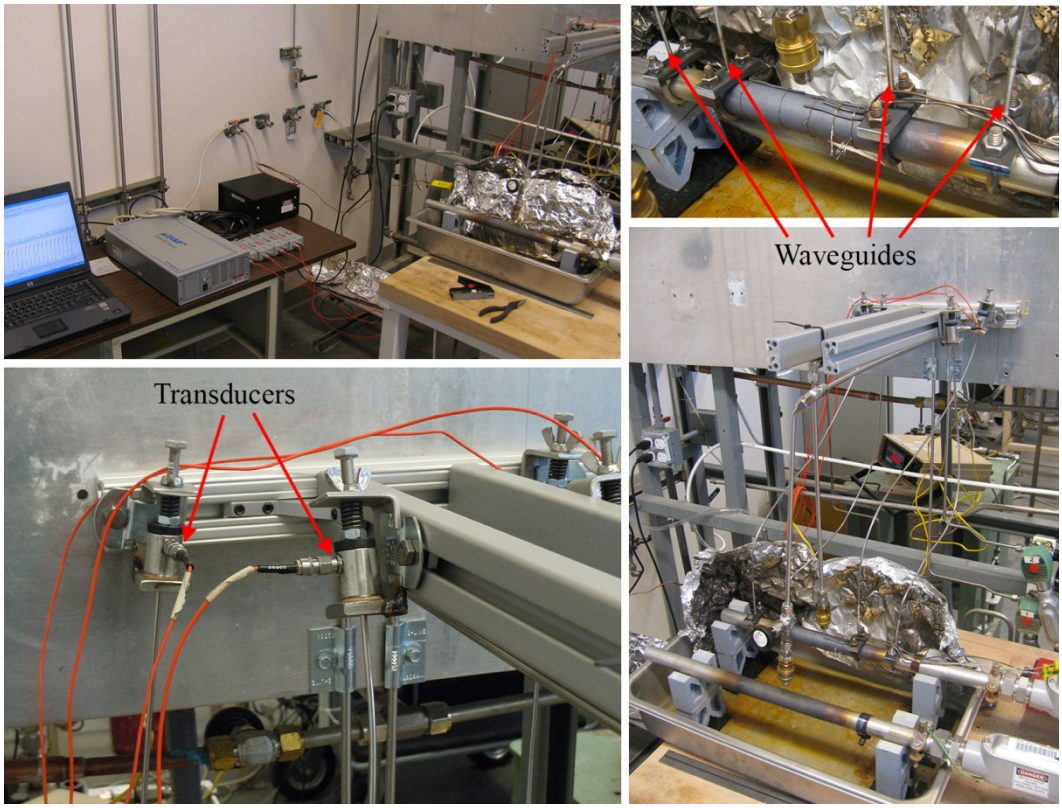


**Figure 3.10**. Photographs of the Thermal Fatigue Experimental Setup and Associated Acoustic Emission Monitoring Equipment

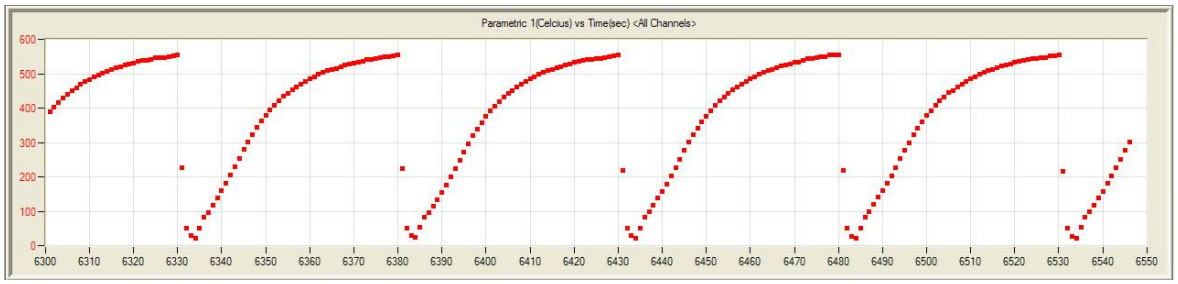


**Figure 3.11**. Example Record of Temperature Cycles Recorded by the Acoustic Emission System

# 4.0 NDE Measurements and Preliminary Analysis Results

## 4.1 Tensile Tests

### 4.1.1 Magnetic Barkhausen Noise

Figure 4.1 presents the averaged peak voltage from the magnetic Barkhausen measurements on a single specimen, at the TOP and BOTTOM locations, as a function of the strain level. The magnetization direction was parallel to the applied strain direction. The specimen failed shortly after the last measurement taken at 24.9% strain. The table also lists the standard deviation at each location (computed from the three measurements at that location), which is a measure of experimental noise.

Figure 4.1 also indicates that the measured MBN voltage increases initially during the elastic strain regime (and perhaps into the plastic strain regime), before decreasing as plastic deformation increases. The table also shows that the measurements from the two locations are generally not similar (within one standard deviation of each other), except at very early stages of degradation. This could be an indication of variability in specimen microstructure and localized variations in processing. It is also likely that variability in the measurement process (manual probe placement) contributed as well. Figure 4.2 shows the average difference between the top and bottom measurements, as well as the mean damage index (DI), which is the average difference normalized to a value between 0 and 1. The normalized differences are also used to compute the standard deviation in the damage index, which is also listed in Figure 4.2.

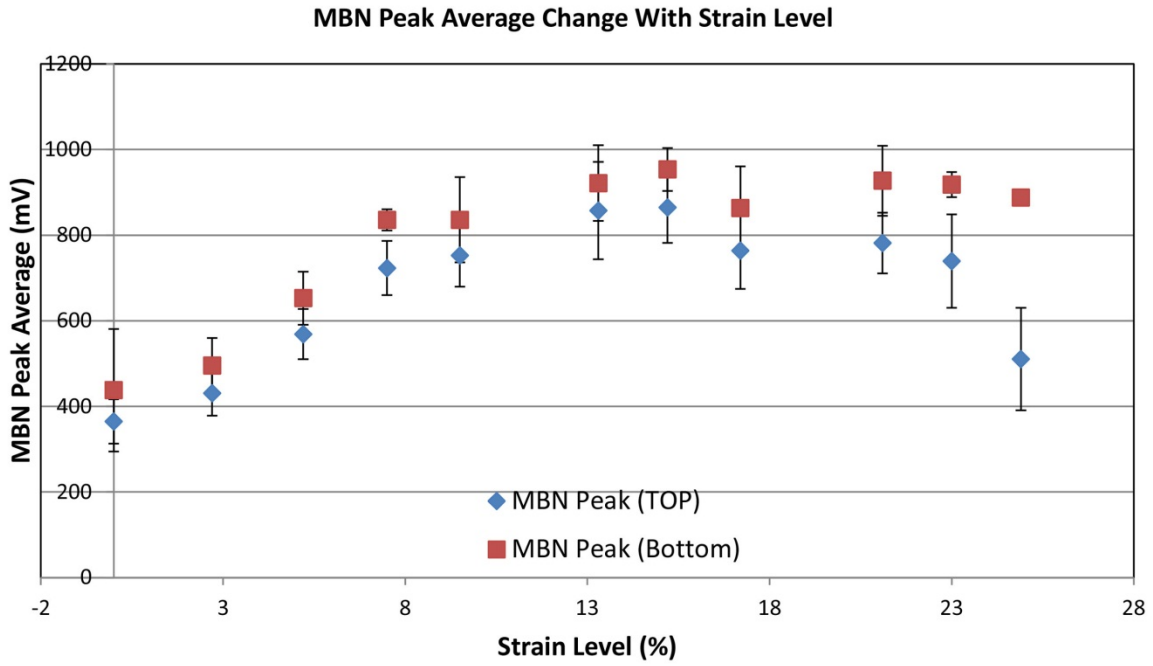


**Figure 4.1**. MBN Peak Average (in mV) as a Function of Strain Level in 410 Grade Steel. Magnetization direction was parallel to applied strain direction.

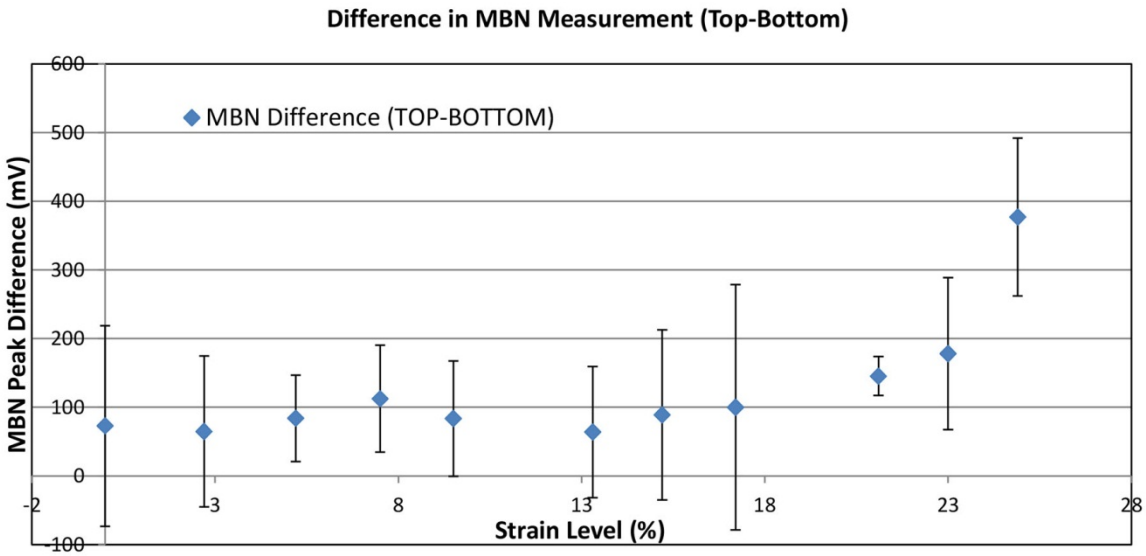


**Figure 4.2**. Difference in MBN Measurements at TOP and BOTTOM Locations on Single Specimen, as a Function of Strain Level

To further evaluate the ability of MBN to identify damage precursor states and identify additional variables that might impact repeatability, measurements were made on a second specimen with the magnetization direction both parallel and perpendicular to the applied strain direction. Figure 4.3 presents the MBN peak for parallel and perpendicular magnetization directions at three locations (TOP, CENTER, and BOTTOM). The difference in behavior of the peak (increasing vs. decreasing trend) with applied strain is likely due to the orientation of the magnetic easy axis and the corresponding impact on the ease of magnetic domain wall movement (Krause et al. 1994; Krause et al. 1995). The data illustrates the need to account for multiple magnetization directions, as well as the potential of using multiple magnetization directions to identify the occurrence of degradation precursors in tensile specimens. However, additional analysis is necessary (using measurements from multiple specimens) to confirm this potential. Probe coupling variability is also seen to contribute to measurement variability, and fixtures that provide reliable, repeatable coupling of the MBN probe are needed. Work to fabricate such fixtures is ongoing and will be tested using the thermal fatigue setup prior to measurements on SCC specimens.

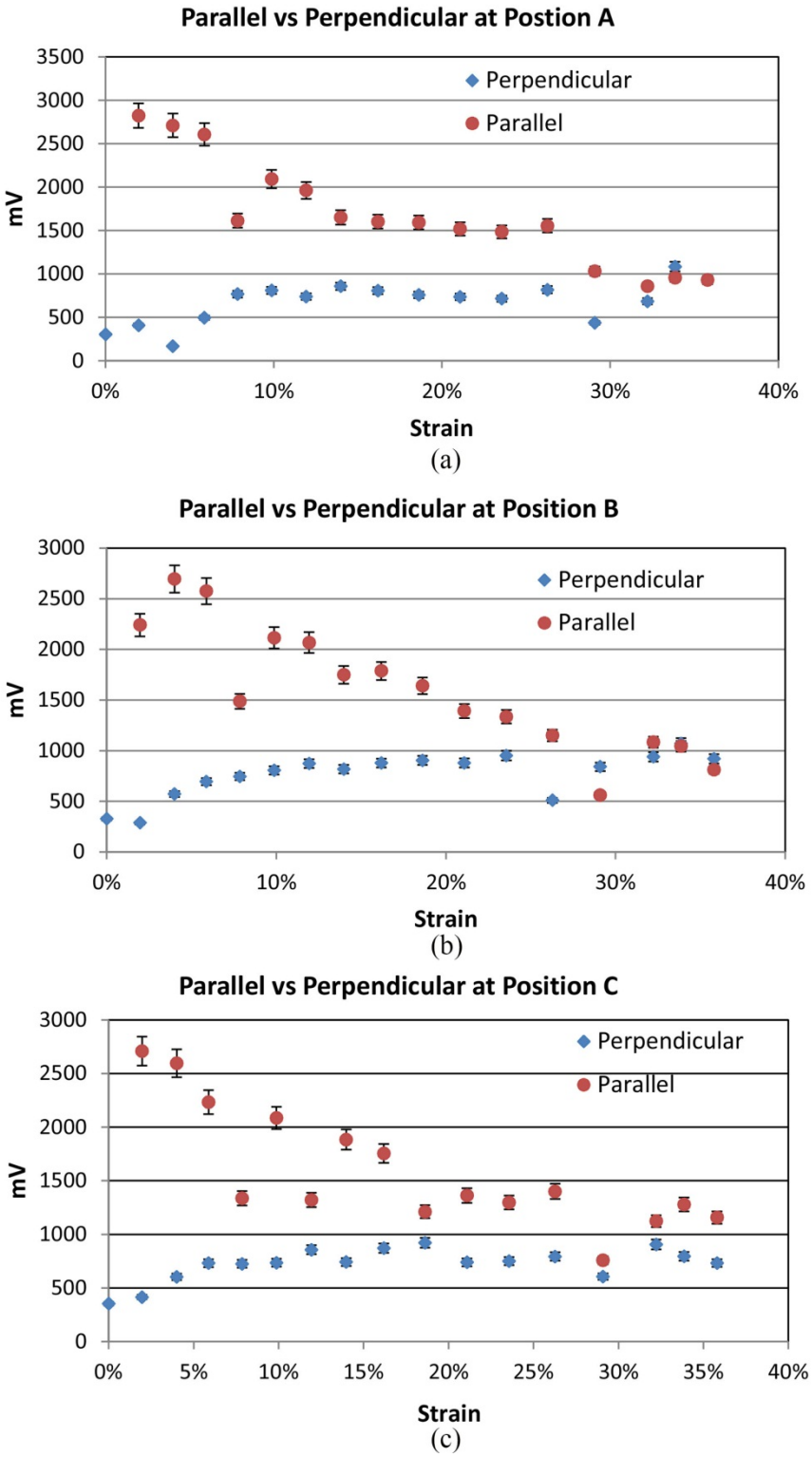


**Figure 4.3**. Impact of Magnetization Direction Relative to Strain Direction on MBN Measurements, as a Function of Applied Strain Level at Three Locations: (a) TOP, (b) CENTER, (c) BOTTOM

### 4.1.2 Acoustic Emission

Traditional AE signal analysis relies on the capture of signal features such as energy, amplitude, duration, rise time, frequency (peak, mean, centroid, etc.), and counts. Material assessment is normally performed by plotting these features versus load parameters or time to identify signatures of failure. Changes in the material are often correlated with points of inflection in cumulative plots of AE activity (hits, counts). Energy and frequency features are assumed to bear a physical relationship with the source of an AE signal and these features are often used to distinguish sources of noise from degradation processes or to distinguish different types of damage mechanisms. Pattern recognition algorithms have been devised to automatically recognize signals exhibiting similar features and group them together. Classification of signal groups could then be performed based on expert opinion and assumptions regarding the nature of signals produced by different source mechanisms. Discrimination of AE signals based on amplitude distributions represents another signal analysis strategy. Several efforts have focused on devising effective means to automate signal clustering and classification to facilitate real-time analysis of signals and minimize measurement ambiguity. Techniques currently under investigation for clustering and classifying AE signals include K-means (Ramadan et al. 2008; Shaira et al. 2008), principle component analysis (Ramadan et al. 2008), and neural networks (Barga et al. 1990). These approaches to analyzing AE signals have evolved because early AE studies focused on small test coupons for which MAE is not applicable (Dunegan 1997).

In the tensile tests, results of location studies from pencil lead breaks, although not accurate for breaks performed near AE sensor 1 and bolt attachment 1, were located consistently and demonstrated that events occurring near the center of the specimen due to deformation should be distinguishable from sources of fretting noise near the sensors and bolt attachments.

The tensile specimens were loaded in 2% strain increments until failure was reached. A significant reduction in coupling was observed (using the auto-sensor tests) at the 12%–14% strain interval, the cause of which is postulated to be deformation (cupping) of the specimen. A dry coupling material was substituted for gel couplant after this interval and consistent coupling was achieved until failure although the dry couplant resulted in approximately 6–9 dB attenuation and, therefore, a loss of sensitivity. Typical results obtained from before and after the couplant change are represented in Figures 4.4 and 4.5. Figures 4.4 and 4.5 represent amplitude of recorded hits (top – in dB) and absolute energy (bottom – aJ) versus time for strain increments from 6%–8% and 16%–18%, respectively. The amplitude and absolute energy of AE signals appears to increase with applied load, indicating the signals are perhaps caused by fretting between the load frame and specimen. No events were recorded by the AE signal processor and at this point it is unclear why the system was unable to locate the source of the signals.

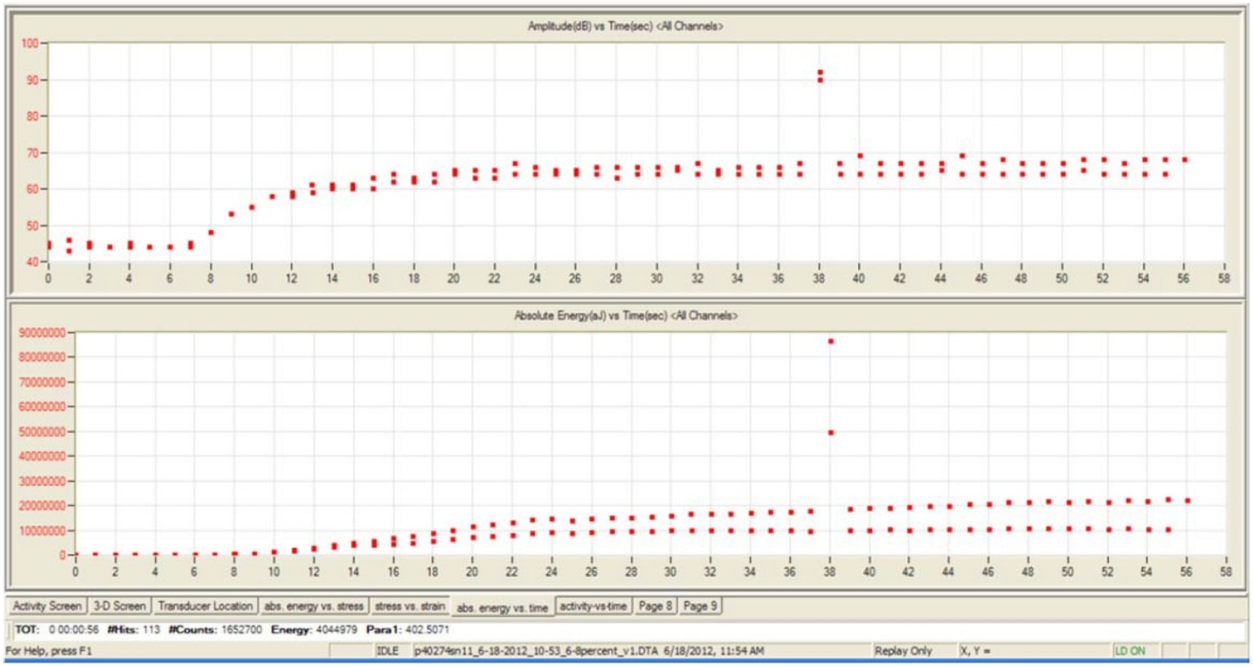


**Figure 4.4**. Screen Capture of the Amplitude of AE Signals (top – dB) and Absolute Energy of AE Signals (bottom – aJ) versus Time for Strain Increment from 6% to 8%

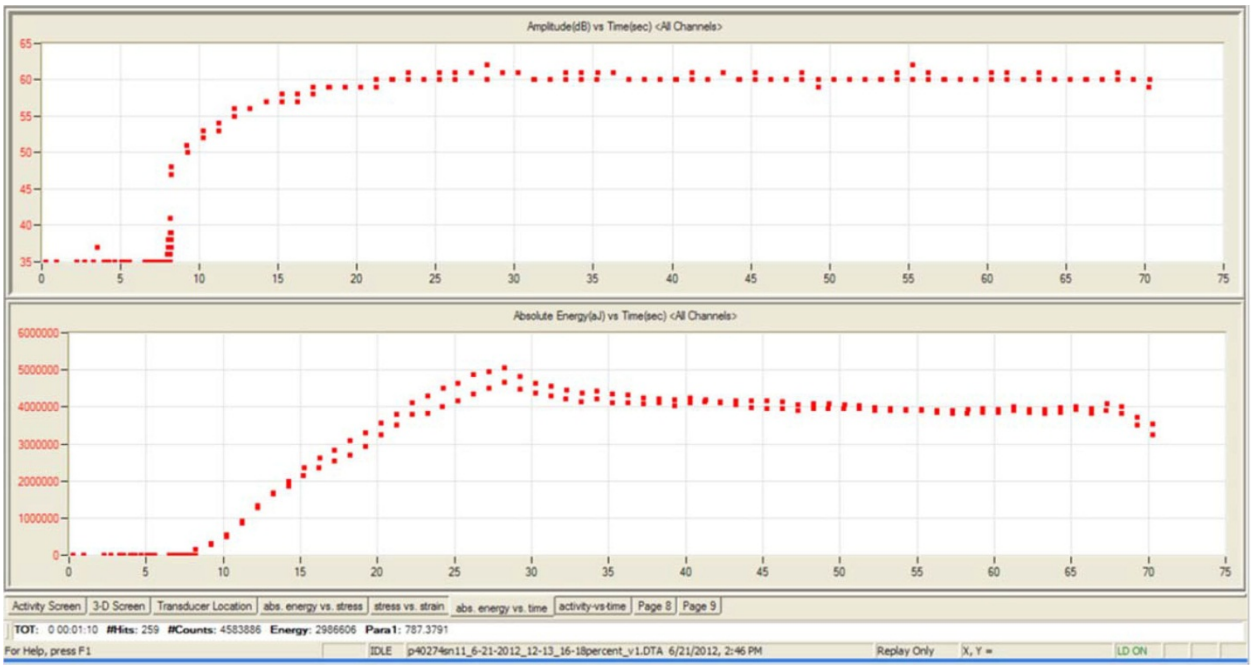


**Figure 4.5**. Screen Capture of the Amplitude of AE Signals (top – dB) and Absolute Energy of AE Signals (bottom – aJ) versus Time for Strain Increment from 16% to 18%

The inability to locate the source of AE activity inhibits efforts to classify its source as noise or degradation. Regardless of the nature of the signals, the accumulation of damage within the specimen will impact the propagation of AE signals. Frequency time plots of individual AE hits have been calculated in an effort to analyze the influence material changes in signal propagation as a result of changes in the material from damage, as shown in Figure 4.6 for signals from the 6% to 8% strain increment and for signals from the 16% to 18% strain increment. Significant differences between the signal characteristics are not obvious from the plots. Potentially, more subtle differences between signals exist and parametric analysis of frequency characteristics will be employed in an attempt to quantify signal changes.

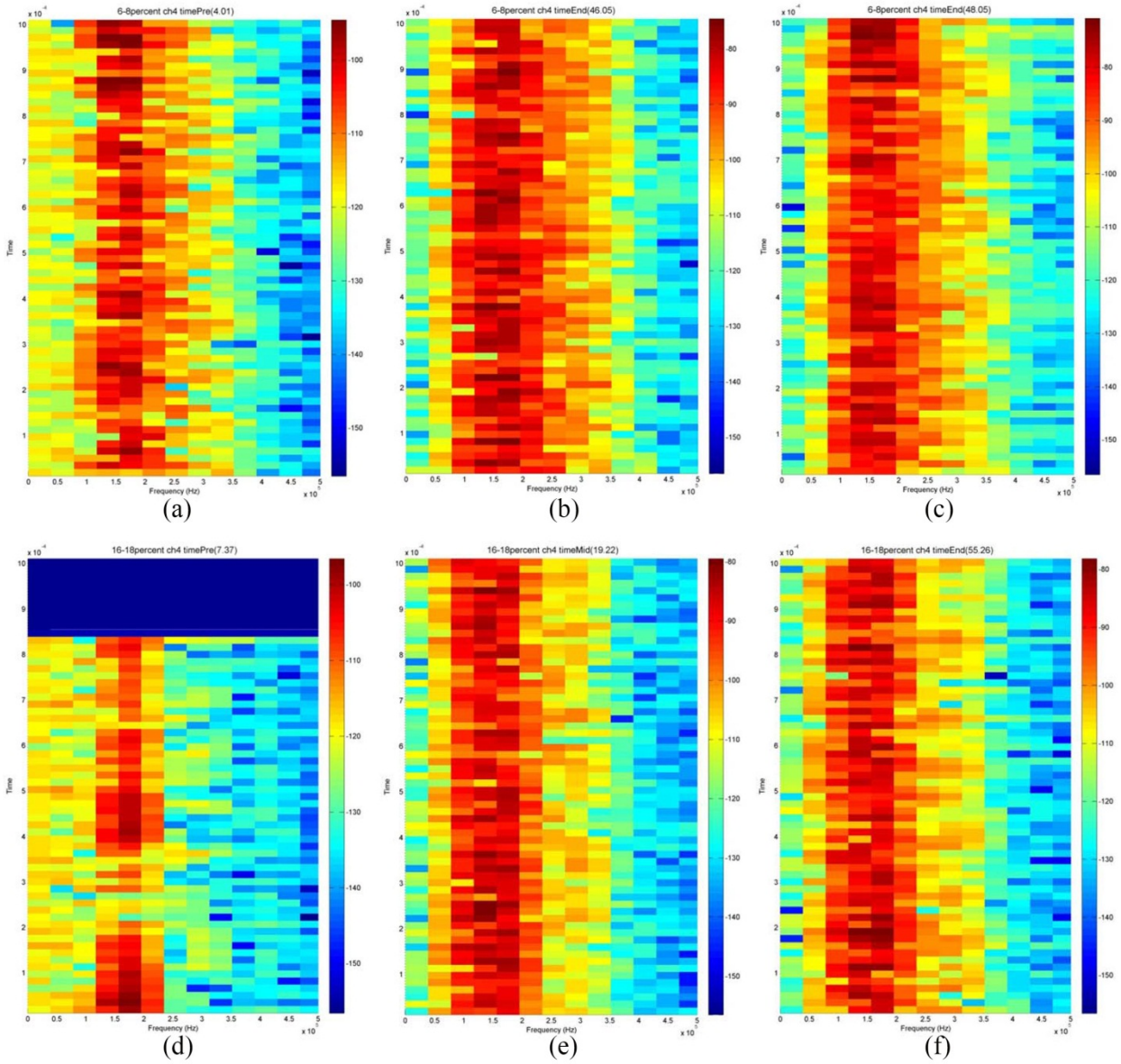


**Figure 4.6**. Frequency – Time Plots of Individual AE Signals Obtained for Strain Increment 6% to 8% at Times a) 4 seconds, b) 14 seconds, c) 48 seconds and for Strain Increment 16% to 18% at Times d) 7 seconds, e) 21 seconds, and f) 55 seconds

### 4.1.3 Nonlinear Ultrasonics

Figure 4.7 presents an example of the recorded data from the two NLU measurement setups. Figures 4.7(a) and (b) show the measured ultrasonic response (A-scan) from the pitch-catch arrangement, at 5 MHz, with an input signal (to the power amplifier) amplitude of 100 mV peak-to-peak (at two different strain levels). Figures 4.7(c) and (d) show similar measurements using the guided wave arrangement. In both cases, a strong fundamental frequency component is seen and any harmonic content is not obvious in the time domain signal. To estimate the nonlinear parameter, the signals were segmented and multiplied by a Hanning window. The resulting signal was analyzed in the frequency domain using the Fourier Transform, and the fundamental and second harmonic amplitudes were measured. The nonlinear parameter β was then computed as:

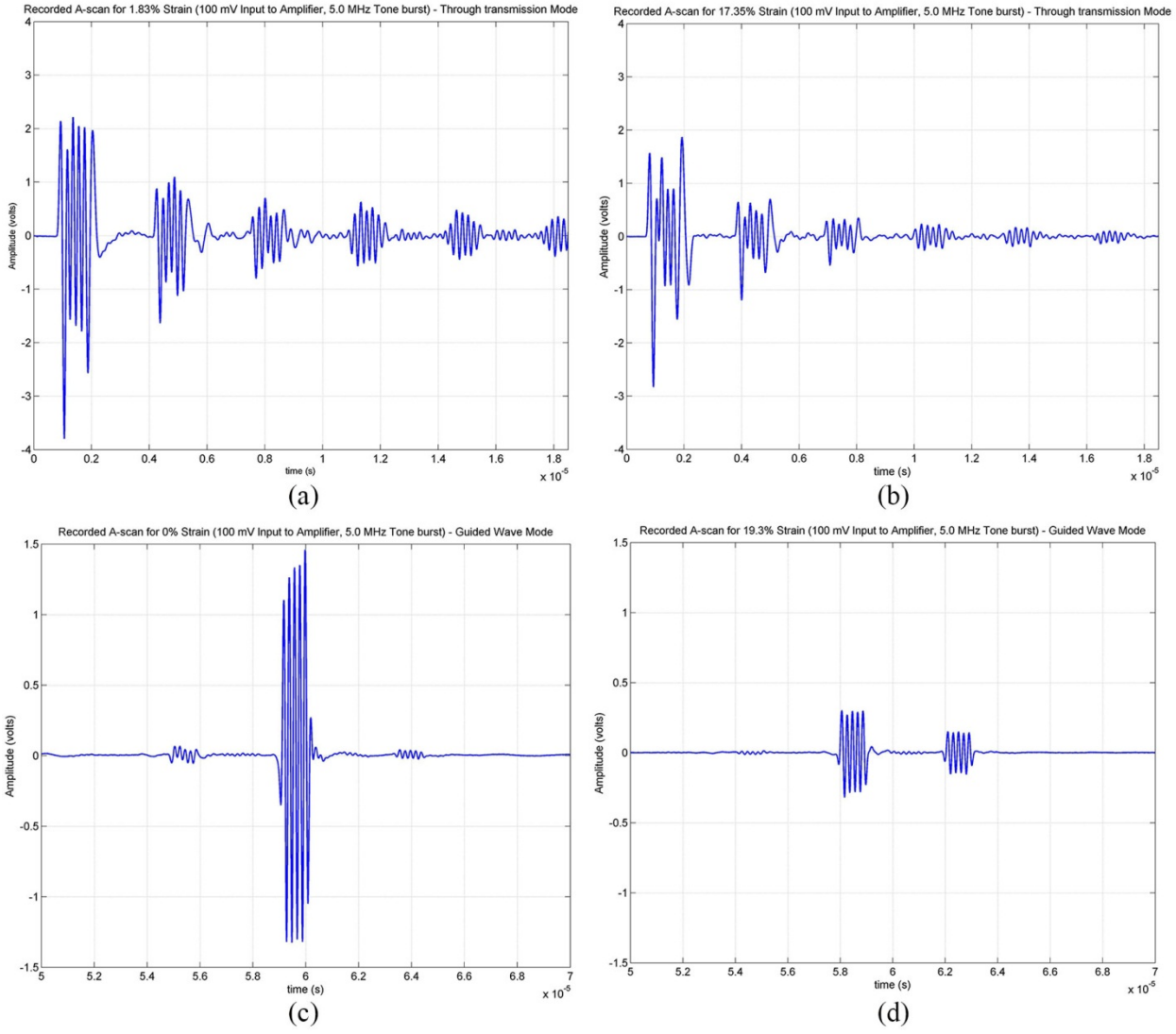


**Figure 4.7**. Examples of A-scans Using Through Transmission and Guided Wave Modes. (a) Through transmission (2% strain), (b) Through transmission (17.83% strain), (c) guided wave mode (0% strain), and (d) guided wave mode (19.83% strain)

$$\beta \propto \frac{A_2}{A_1^2} \tag{4.1}$$

where the constant of proportionality depends on the frequency, material elastic properties, and whether the measurement is made using a longitudinal wave, surface wave, or lamb wave (Bermes et al. 2008). In both measurement arrangements, the entire signal was used to compute the second harmonic as well as the fundamental frequency component. The calculation was repeated for all frequencies and all input voltage levels, at each strain level. To ensure that data was properly normalized, the measurement from the annealed specimen (0% strain) was used to calculate a normalizing value of $\beta$ (called $\beta_0$). Note that $\beta_0$ varied according to frequency and input voltage. The calculated value of $\beta$ at any frequency and input voltage level was normalized using the corresponding $\beta_0$ as follows:

$$\beta_n = \frac{\beta}{\beta_0}. \tag{4.2}$$

The normalized nonlinear parameter $\beta_n$ at each frequency and strain level was then averaged over all input voltage levels, and the standard deviation calculated.

Figure 4.8 presents the normalized nonlinear parameters as a function of strain level for the through-transmission approach, while Figure 4.9 presents similar measurements for the guided wave arrangement. In both figures, the parameter computed from each of the three excitation frequencies is presented (using a logarithmic scale). As seen from the data in Figure 4.8, the NLU parameter is seen to be relatively stable initially. As the sample approached irreversible plastic damage (and started necking) around 12-15% strain, the parameter is seen to increase. However, the standard deviation in the measurement (which is a measure of error) is also seen to increase significantly. The normalized nonlinear parameter $\beta_n$ is also seen to exhibit multiple peaks past this point. Examination of the specimen indicated that some of the instability in the measurement after this stage was probably due to significant surface deformation resulting in insufficient coupling of the ultrasonic probes in the transmit-receive arrangement. However, the measurement is still seen to trend upwards until failure, indicating that addressing the coupling issue could result in a significantly sensitive method to measure microstructural changes prior to failure.

Figure 4.9 shows the result of using the guided wave arrangement (for all three excitation frequencies) on a second specimen, to ensure that the probes are sufficiently separated from the region of plastic deformation, thereby ensuring adequate coupling of the probes. However, this arrangement results in the need to perform a dispersion analysis to determine the likely modes of propagation of the applied energy. As seen from Figure 4.10, while the incident energy may be at 4.5 MHz (or 5 MHz, or 5.5 MHz), the finite bandwidth of the transducer implies that a range of frequencies are likely to be propagating in the material. Similarly, guided wave analysis indicates that a finite aperture for the probe will result in a phase velocity bandwidth that defines the possible mode structures that are excited in the material. These two bandwidth parameters define the mode structures that form the incident energy mode profile. As this energy propagates along the waveguide (specimen), damage in the material results in the generation of harmonics. In the present case, the harmonic content is not controlled and the resulting harmonic frequency content will not be cumulative (Bermes et al. 2008) (i.e., one or more harmonic modes will be generated that have differing phase velocities from each other and the incident modes). The resulting harmonic content from different locations in the material will therefore arrive at the receiver at different times. Note that this can be avoided by careful selection of the fundamental and harmonic modes such

that they both have the same group velocity. In this special case, the harmonic frequency generation is cumulative as the fundamental frequency component propagates along the structure, and both modes arrive at the receiver at the same time. In the present case, such a choice is complicated by the fact that, as the specimen is strained, the dimensions of the gauge section change, resulting in a shift in the operating point on the dispersion curves. This changes the mode structure and destroys any coherency there may have been initially.

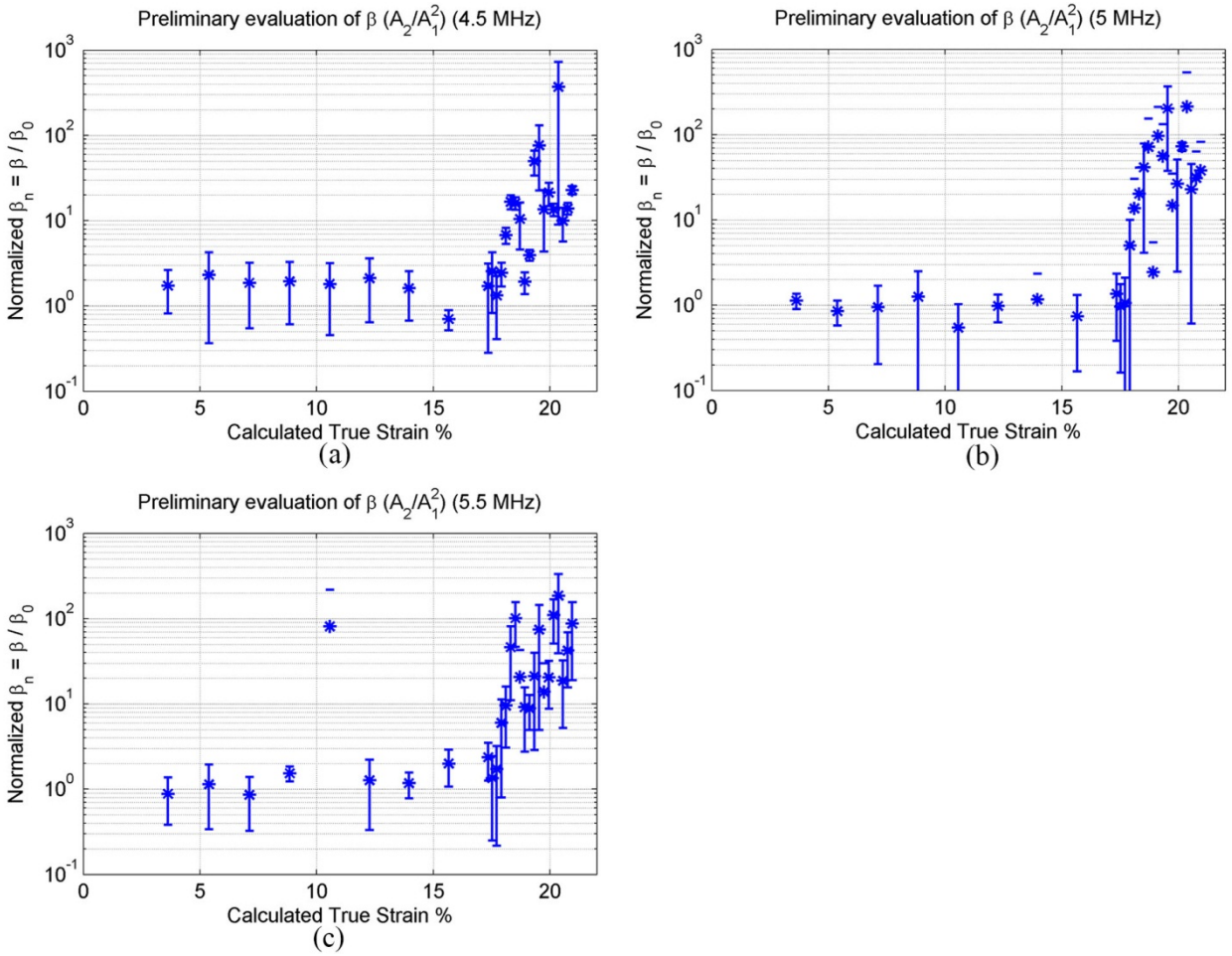


**Figure 4.8**. Normalized Nonlinear Parameter Computed Using Through Transmission Mode as a Function of Applied Strain, with Ultrasonic Incident Frequency (a) 4.5 MHz, (b) 5 MHz, and (c) 5.5 MHz

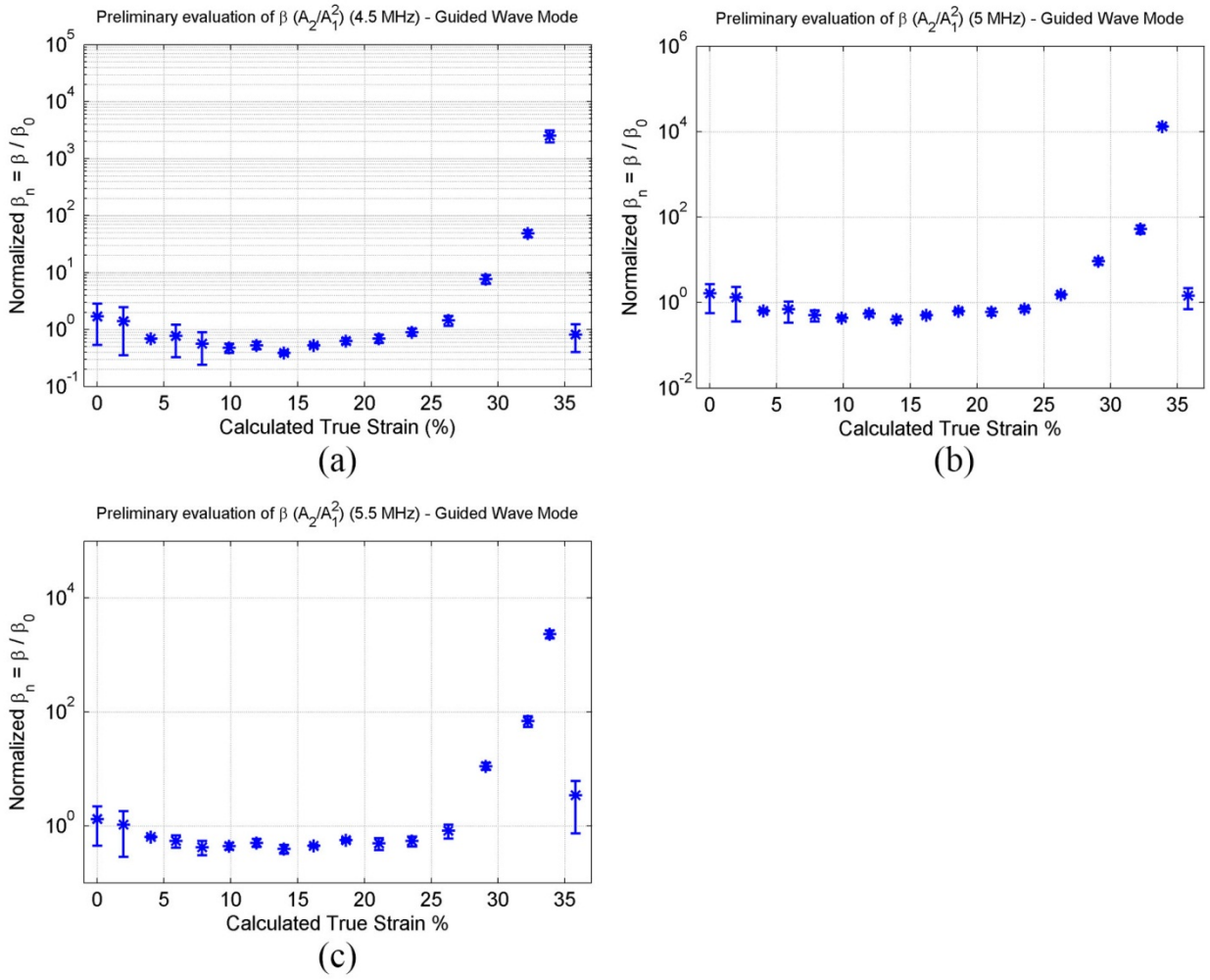


**Figure 4.9**. Normalized Nonlinear Parameter Computed Using Guided Wave Mode as a Function of Applied Strain, with Ultrasonic Incident Frequency (a) 4.5 MHz, (b) 5 MHz, and (c) 5.5 MHz

In the present case, the harmonic modes are expected to arrive at different times, and the resulting nonlinear parameter (suitably normalized) is seen to trend strongly with accumulated damage in the material (Figure 4.9).

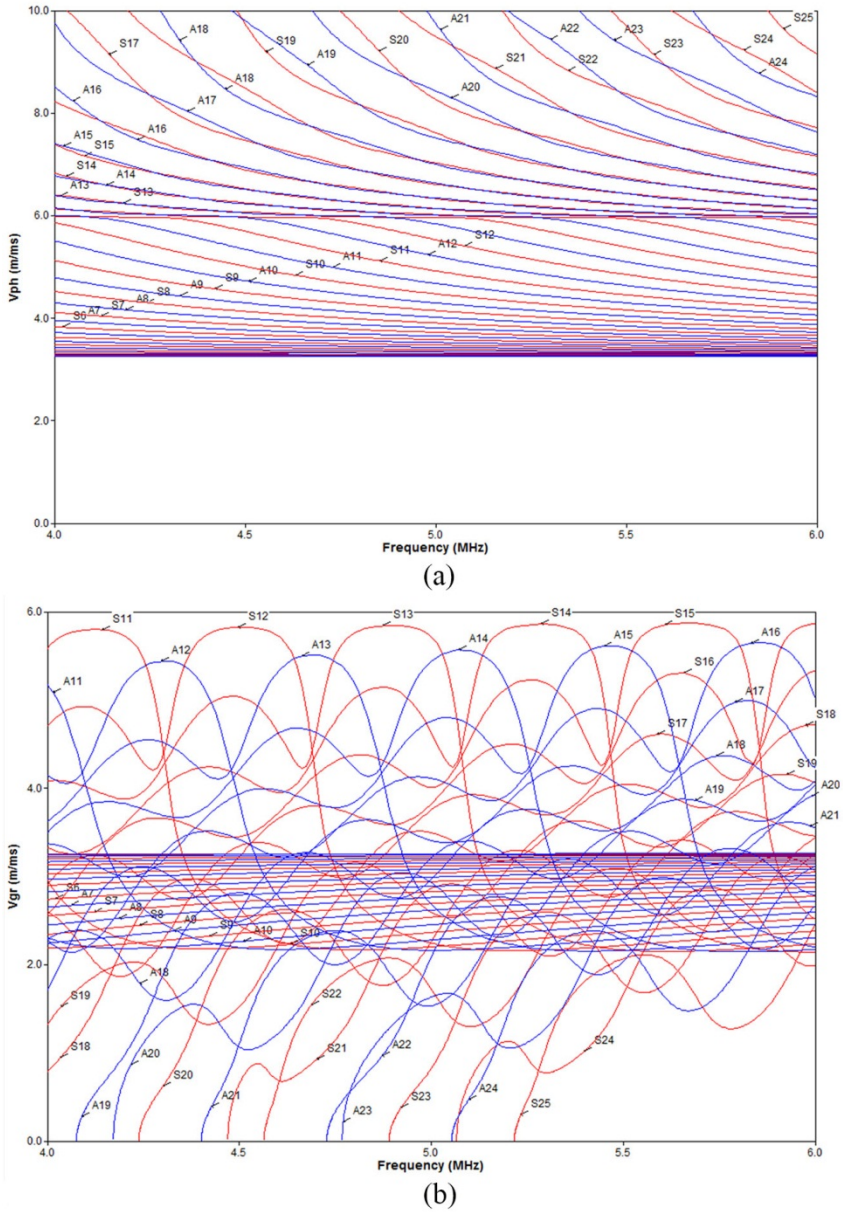


**Figure 4.10**. Dispersion Analysis in the 4 MHz–6 MHz Frequency Band for a 10-mm-thick Steel Plate: (a) phase velocity diagram, (b) group velocity diagram

## 4.2 Thermal Fatigue

### 4.2.1 Magnetic Barkhausen Noise

Preliminary measurements were taken on a thermally fatigued specimen, after crack initiation, to determine if measurable micromagnetic changes occur in the material under consideration after crack initiation. Measurements were made at a 125-Hz repetition rate with a 5-volt peak-to-peak excitation signal. Magnetic Barkhausen signals were acquired over the 70–200-kHz frequency range. The magnetic

Barkhausen emissions tests show promising results as the peak signals change in the fatigued area compared to the undamaged ends of the steel rod (Figure 4.11). This indicates a potential variation in micromagnetic measurements (for 304SS) with the degree of thermal aging and fatigue damage accumulation that can potentially be exploited to measure precursors to such degradation mechanisms. However, the sensitivity of the measurements needs quantification, as does correlation of the measurements to physical damage in the material (which can be quantified using destructive analysis of the specimen).

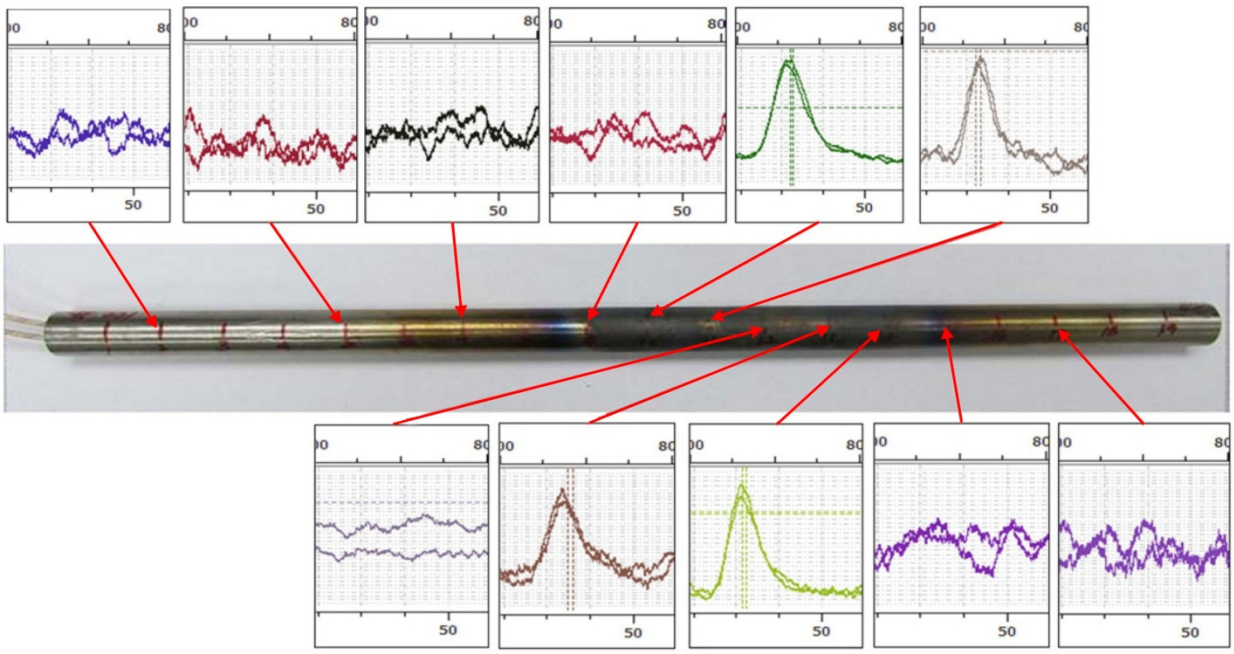

**Figure 4.11**. MBN Data Taken Along the Length of a Thermal Fatigue Specimen with a Crack at the Center of the Specimen

### 4.2.2 Acoustic Emission

Acoustic Emission data has been collected on a single specimen thermally cycled until cracking was observed visually near 8000 cycles. A rearrangement of the waveguides was conducted at 2670 cycles, and so the data prior to this rearrangement is excluded from the following analysis. The specimen was thermally cycled in a series of intervals between which the test was paused to allow for other NDE measurements and to check the integrity of waveguide coupling with the specimens. Following the seventh interval, the AE system "froze" and failed to collect data during 600 thermal cycles. The AE system was restarted at the beginning of the next interval, which is referred to as interval 8, and performed satisfactorily until failure was observed during interval 10. A brief summary of the cycling intervals and AE data is provided in Table 4.1. The "freezing" of the AE system is indicated by the shaded blue row in Table 4.1. In addition, Table 4.1 also indicates a thermocouple failure at the beginning of interval 5, which is shaded green. This is significant because replacement of the thermocouple could lead to a slight rearrangement of the thermocouple on the surface of the specimen.

**Table 4.1**. Summary of AE Data Collected Over Several Thermal Fatigue Intervals Spanning the Specimen Lifetime Beyond 2670 Cycles. Interval 5 is shaded green to highlight thermocouple failure and replacement at the beginning of the interval. No AE data was collected between intervals 7 and 8 (highlighted light blue), and cracking was visual observed during interval 10 (orange highlight).

| Interval | Cycles | Cumulative Cycles | Total Hits | Total Energy | Hits/Cycle | Energy/Hit |
|---|---|---|---|---|---|---|
| 1 | 486 | 3156 | 141223 | 5.50E+10 | 290 | 3.89E+05 |
| 2 | 522 | 3678 | 219286 | 7.00E+10 | 420 | 3.19E+05 |
| 3 | 498 | 4176 | 94648 | 3.50E+10 | 190 | 3.70E+05 |
| 4 | 1200 | 5376 | 269136 | 1.10E+11 | 224 | 4.09E+05 |
| 5 | 222 | 5598 | 52313 | 1.85E+10 | 235 | 3.54E+05 |
| 6 | 210 | 5808 | 39613 | 1.40E+10 | 188 | 3.53E+05 |
| 7 | 90 | 5898 | 14144 | 1.40E+10 | 157 | 9.90E+05 |
| --- | 600 | 6498 | --- | --- | --- | --- |
| 8 | 396 | 6894 | 75010 | 7.80E+10 | 189 | 1.04E+06 |
| 9 | 1122 | 8016 | 256917 | 2.25E+11 | 228 | 8.76E+05 |
| 10 | 306 | 8322 | 64446 | 4.80E+10 | 210 | 7.45E+05 |

#### 4.2.2.1 Results with Frequency Filtering (fc > 190 kHz)

Frequency filtering was initially applied in an attempt to separate out background AE signals by specifying a cutoff centroid frequency (fc) of 190 kHz. Signals with fc greater than this cutoff were attributed to degradation while signals below this cutoff were attributed to the background contributed by the environment. The absolute energy spectrum for the higher frequency signals (> 190 kHz) collected during interval 1 is shown in Figure 4.12. In addition, the AE activity is plotted over six thermal cycles in intervals 1 and 9 to observe the relationship between the emission of signals with fc greater than and less than 190 kHz. These plots are provided in Figures 4.13 and 4.14, respectively. Finally, the activity of AE signals with fc > 190 kHz is provided in Figure 4.15 in terms of hits per thermal cycle and cumulative AE hits. This information is over-laid on bars indicating the average and standard deviation of this AE activity for each cycling interval.

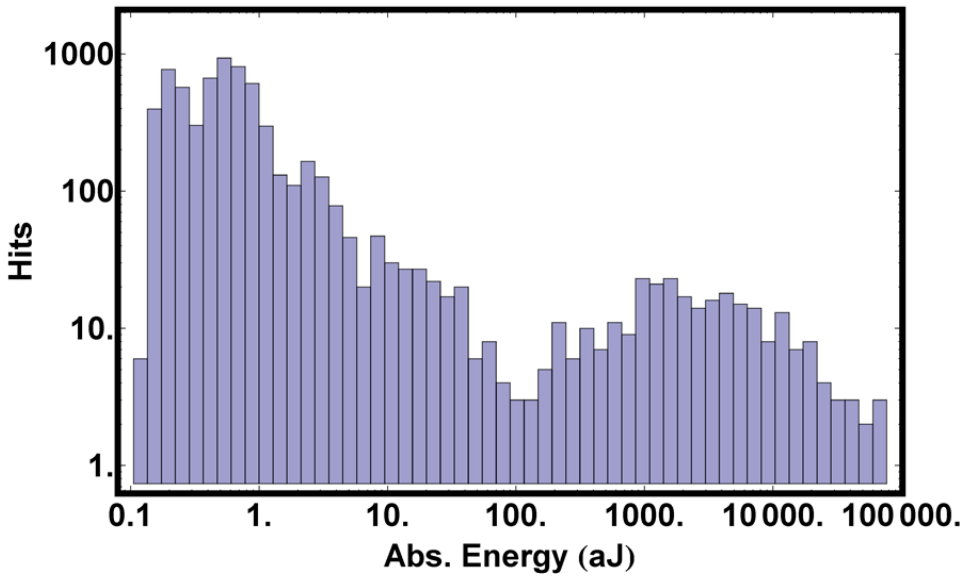


**Figure 4.12**. Energy Spectrum of Background Signals (< 190 kHz) Collected During Interval 1

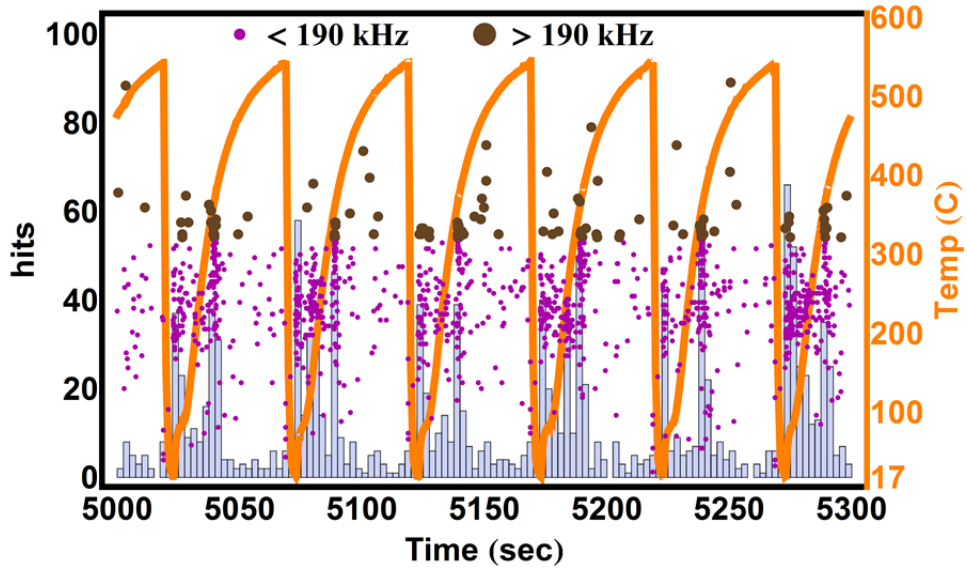


**Figure 4.13**. AE Activity Collected Over Six Thermal Cycles During Interval 1 Along with a Plot of the Thermocouple Signal During These Cycles; Signals with Centroid Frequency Greater Than 190 kHz are Highlighted Using Enlarged Dots

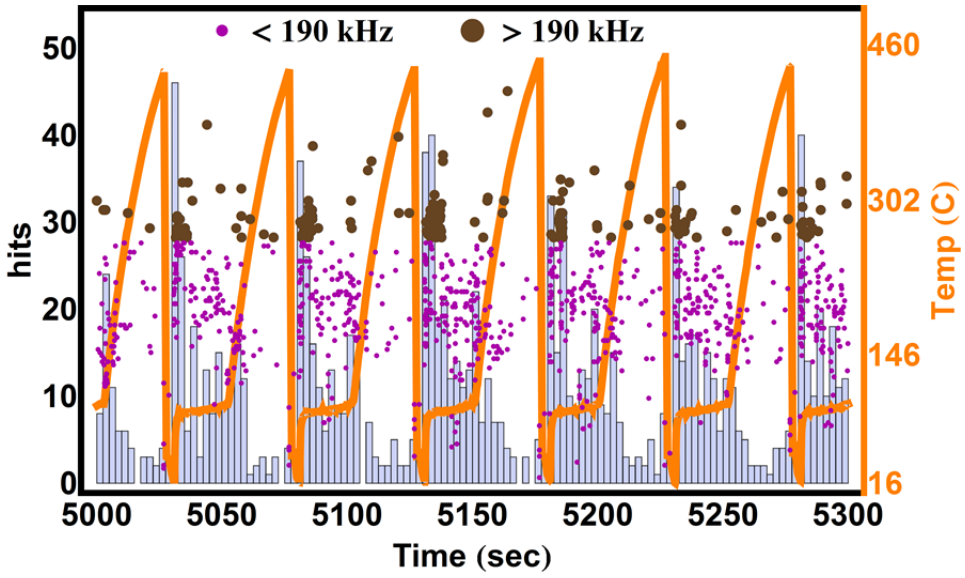


**Figure 4.14**. AE Activity Collected Over Six Thermal Cycles During Interval 9 Along with a Plot of the Thermocouple Signal During These Cycles; Signals with Centroid Frequency Greater Than 190 kHz are Highlighted Using Enlarged Dots

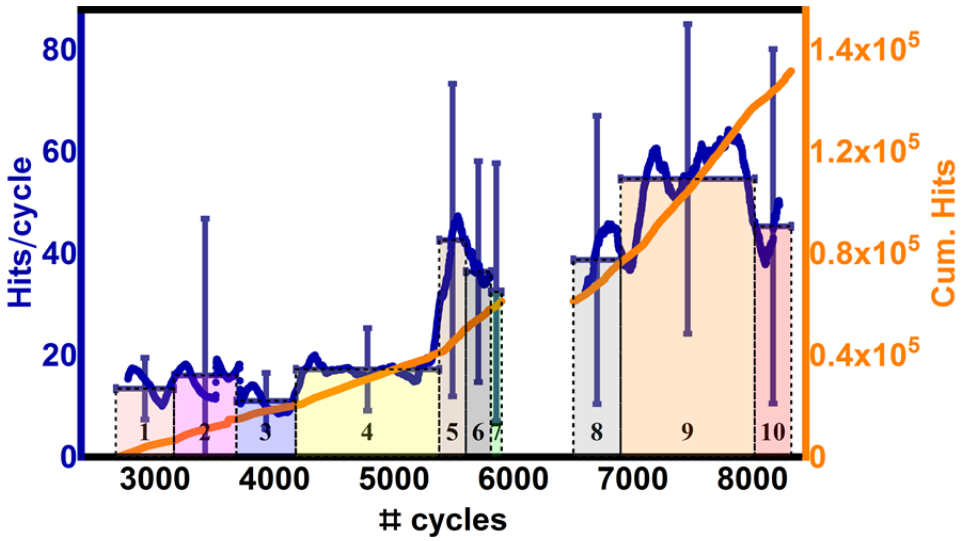


**Figure 4.15**. Summary of the Activity of AE Signals with Centroid Frequency Greater Than 190 kHz Over the Lifetime of the Specimen

#### 4.2.2.2 Results with Frequency (> 190 kHz) and Energy Filtering (5–100 aJ)

Next, an energy filter was applied on top of the frequency filter in an effort to further discriminate environmental sources of AE. The energy spectrum of signals with centroid frequency greater than 190 kHz is provided in Figure 4.16 for intervals 1 and 10 (labeled as "3000 cycles" and "8000 cycles," respectively). Figure 4.16 indicates significant overlap between the two spectrums with a couple of exceptions, the most significant of which occurs over the energy range of approximately 1–100 aJ with interval 10 exhibiting a much greater number of hits in this energy range than interval 1. AE activity over a handful of cycles during interval 9 is plotted along with the thermocouple signal and displayed in Figure 4.17. Also in Figure 4.17 is a plot of when hits both above and below 190 kHz occur within these cycles, with hits above 190 kHz also subject to the energy window. Finally, with both centroid frequency and energy filters applied, AE activity in terms of hits/cycle and cumulative hits is plotted from interval 1 to interval 10 in Figure 4.18.

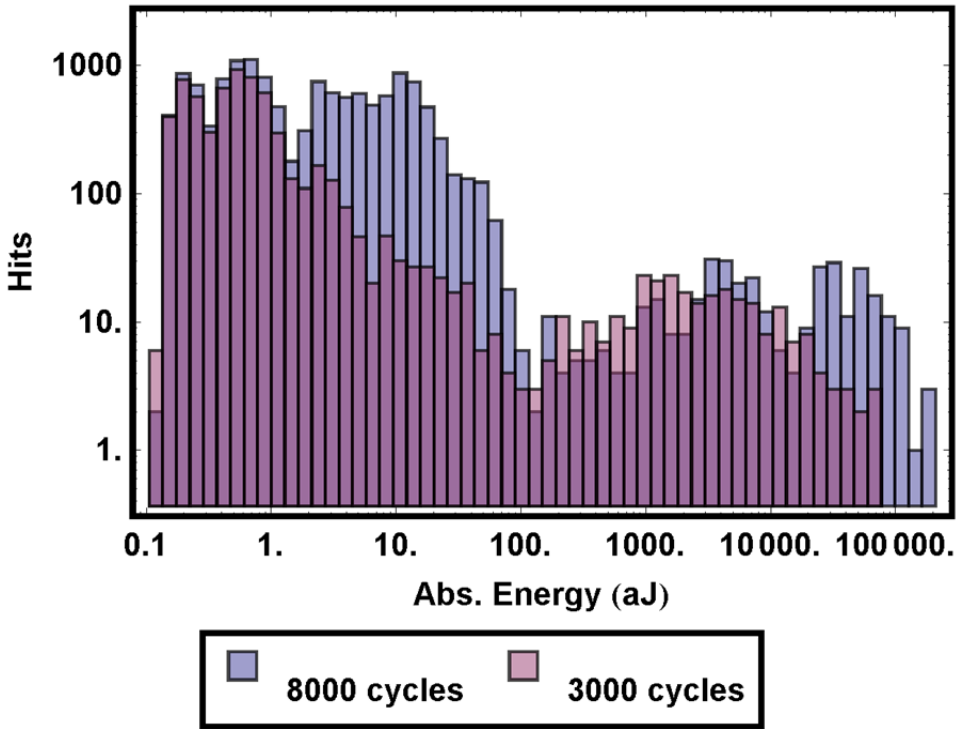


**Figure 4.16**. Energy Spectrum of Signals with Centroid Frequency Greater Than 190 kHz for Intervals 1 and 10

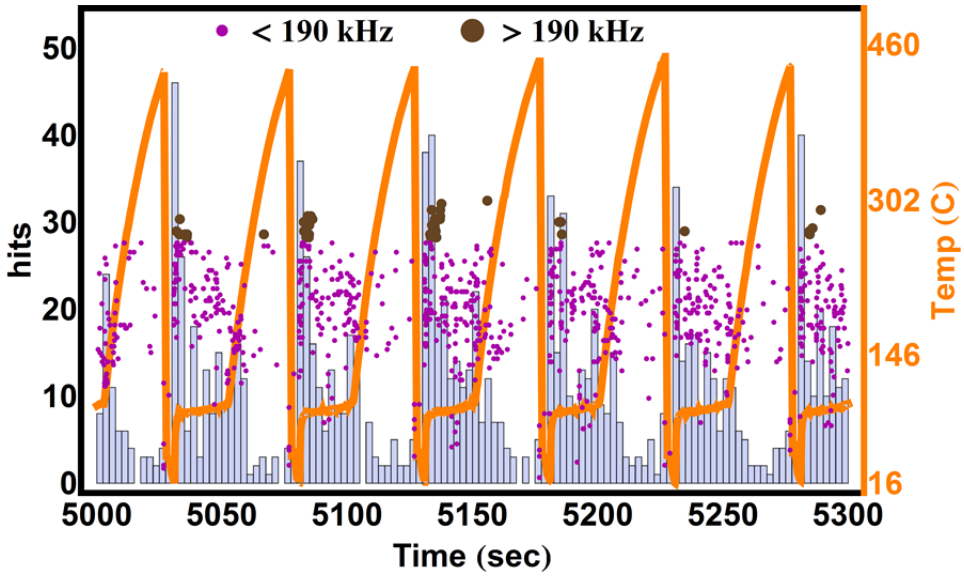


**Figure 4.17**. AE Activity Over a Handful of Cycles During Interval 9 Plotted along with the Thermocouple Signal to Illustrate when Signals Above and Below 190 kHz Occur Within a Thermal Cycle

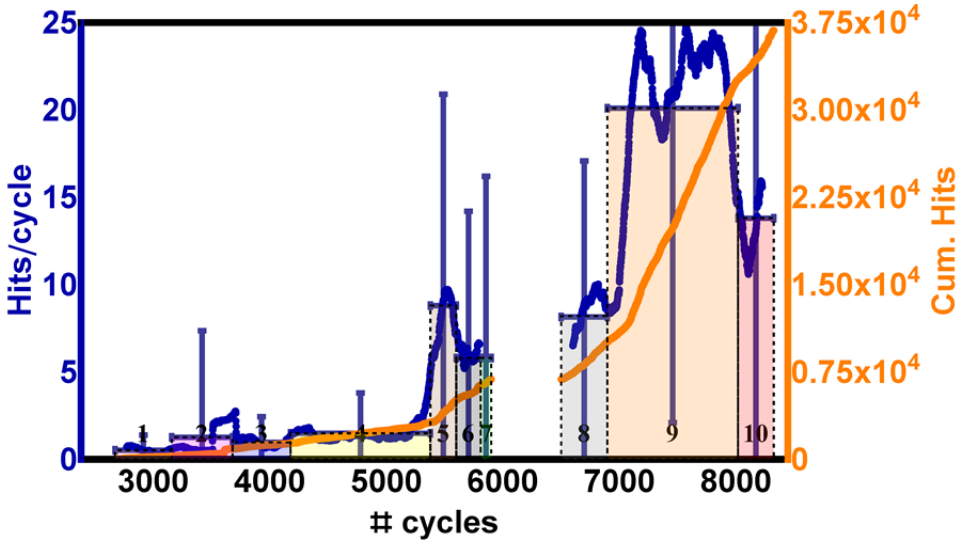


**Figure 4.18**. AE Activity in Terms of Hits/Cycle and Cumulative Hits is Plotted from Interval 1 to Interval 10 with Both Centroid Frequency (> 190 kHz) and Energy Filters (5–100 aJ) Applied

### 4.2.3 Characterization of Remaining Signals

The energy spectrum of background signals is provided in Figure 4.19 and the AE activity associated with the background is provided in Figure 4.20 for the thermal fatigue intervals in Table 4.1. The background is determined as those signals that are excluded by the combined frequency and energy filters. The AE activity is represented as hits/cycle and cumulative hits throughout the monitored lifetime

of the specimen. The activity is fairly constant over the life of the system, which is consistent with expectations for activity from a background source.

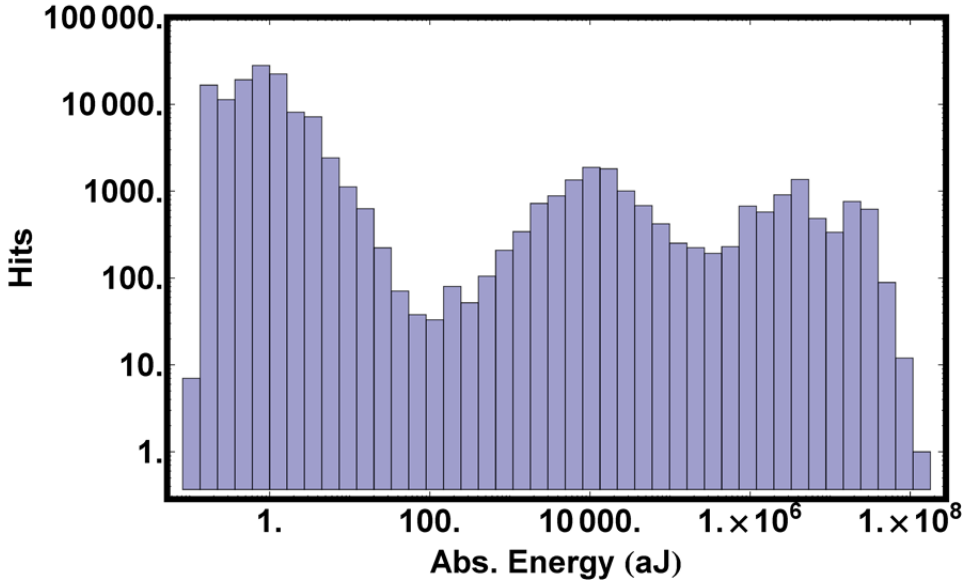


**Figure 4.19**. Energy Spectrum of the Remaining AE Signals in Interval 1 to Interval 10 After Removing Signals with Centroid Frequencies Greater Than 190 kHz and Energies in the Range of 5 aJ–100 aJ

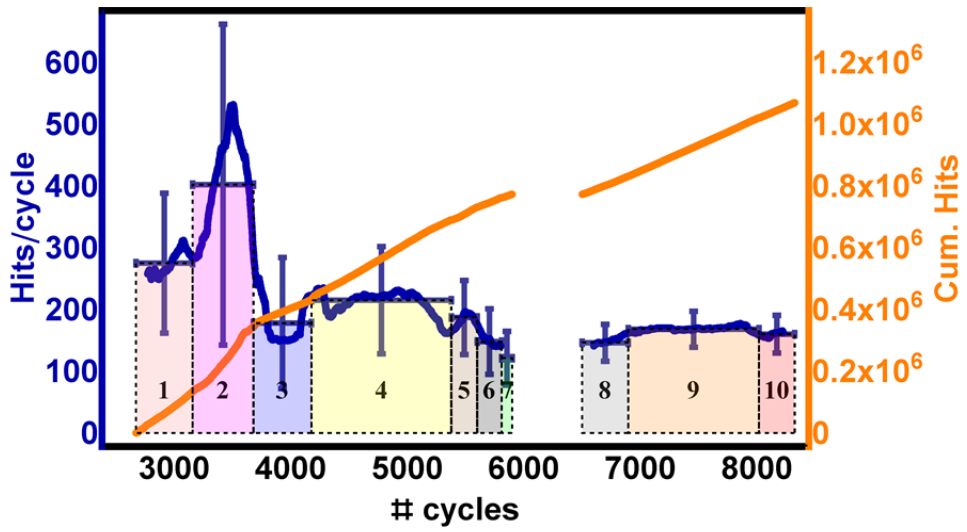


**Figure 4.20**. AE Activity of the Remaining Signals in Interval 1 to Interval 10 After Removing Signals with Centroid Frequencies Greater Than 190 kHz and Energies in the Range of 5 aJ–100 aJ

### 4.2.4 Discussions

The trend observed in Figure 4.18 is encouraging and agrees with early damage evolution through the accumulation of material inhomogeneities. The large standard deviations observed are consistent with discontinuous or burst-like emissions that are often associated with certain forms of degradation such as cracking (Harris and Dunegan 1974). In Figure 4.15, the observed trend still exhibits general behavior in line with expectations from damage accumulation, but the trend is much weaker and indicates that signal analysis based only on the centroid frequency parameter may be insufficient for discrimination of damage signals from signals originating from the external sources. Given the results observed in Figure 4.18, it is important to interpret the data with respect to material condition. Specifically, there is a need to conclusively determine if there are any features in the AE data that are indicators of crack initiation and if the stage of degradation can be inferred from AE behavior. The data evaluated in this limited study is insufficient to make conclusive determinations. True-state measurements are required to determine whether AE behavior can be applied to estimate the degradation state. Further, analysis of the response of several specimens is needed so that conclusions regarding the interpretation of AE behavior can be made with high confidence. Both of these steps are planned in future efforts.

Additional refinements to the system are planned as well. As mentioned above, replacement of a thermocouple at the beginning of interval 5 resulted in trapping water on the surface of specimens and subsequent boiling. This boiling introduced a source of AE signals for intervals 5–10 that was not present in intervals 1–4. The amount of influence this has on observed trends in the AE data is not known. The thermocouple replacement is coincident with the observation of a significant increase in AE activity in Figure 4.15 and Figure 4.18. On the other-hand, significant increases in AE activity are observed during later intervals that appear to be independent of thermocouple repositioning. In addition, the relative increase in acoustic noise after thermocouple replacement due to boiling is not known. The data in Figure 4.17 indicates that signals included in Figure 4.18 are consistently emitted just after the cooling period and appear clustered in only a brief moment during the entire thermal cycle, whereas boiling is clearly present over a much larger portion of the thermal cycle. This AE behavior is consistent with expectations of signals emitted by degradation, which would occur at moments of greatest stress concentration during the thermal cycle. It is still possible that the observed signals are associated with only a certain stage of boiling, such as nucleate boiling; therefore, boiling cannot be ruled out as a potential source for these signals.

In addition to boiling, the relative positioning of specimens and the water spray could influence AE response over specimen lifetime if the relative positioning is shifted. The uncertainties caused by boiling and relative positioning of water spray and specimen can be minimized. This will be the focus of planned refinements to the system. Other refinements will focus on minimizing sources of fretting and potentially using wide-band sensors to enable potentially more robust discrimination of noise and degradation signals based on frequency response.

## 4.3 Next Steps

An analysis of the results to date indicates that MBN and NLU measurements exhibit good correlations with accumulated damage in materials. However, both measurements are sensitive to a number of factors, including probe coupling, orientation of the probe (for MBN) relative to the strain direction, measurement technique (for NLU), initial material microstructure, and measurement location or region. These factors will need to be addressed before additional measurements may be made to characterize SCC precursors, especially if these measurements will have to be made in situ. The factors impacting measurements also affect data collected from the thermal fatigue setup (next), and a mechanical fixture to control positioning and coupling in a repeatable manner is being fabricated prior to additional measurements. While AE has been shown in the literature to be a viable choice for in-situ monitoring of degradation accumulation, the results to date have demonstrated the need for a robust set of algorithms for analysis of the AE data, to enable rejection of any external noise sources while enhancing the AE response from mechanisms of interest. These findings will be addressed in the next phase of the project.

# 5.0 Summary and Future Work

The ability to measure the accumulation of degradation in reactor materials, through nondestructive methods that are sensitive to degradation precursors, will be important in efforts towards extending the life of operational LWRs. During the current phase of this project, potential NDE measurement methods were evaluated on prototypical degradation mechanisms (mechanical and thermal fatigue). Multiple measurement methods were evaluated and variables that impact the measurement accuracy and reliability were identified and addressed. The selected measurement methods show promise, with sensitivity to early stages of material degradation and cracking precursors. Additional confirmatory measurements with thermal and mechanical fatigue are expected to be completed shortly. Destructive analysis, including optical metallography and electron backscatter diffraction (EBSD) measurements on the aged materials are necessary to identify specific microstructural features that may be responsible for the measurements. These are expected to be completed in early FY13, along with beginning evaluations of the selected NDE methods for the detection of SCC precursors.

# 6.0 References


10 CFR 50.55a. 2007. "Codes and Standards." Code of Federal Regulations, U.S. Nuclear Regulatory Commission, Washington, D.C. Available at http://www.nrc.gov/reading-rm/doc-collections/cfr/part050/part050-0055a.html.

Alvarez MG, P Lapitz and J Ruzzante. 2008. "AE Response of Type 304 Stainless Steel During Stress Corrosion Crack Propagation." *Corrosion Science* 50(12):3382-3388.

Andresen PL, FP Ford, K Gott, RL Jones, PM Scott, T Shoji, RW Staehle and RL Tapping. 2007. *Expert Panel Report on Proactive Materials Degradation Assessment*. NUREG/CR-6923, BNL-NUREG-77111-2006, U.S. Nuclear Regulatory Commission, Washington, D.C.

ASNT. 2004. *Nondestructive Testing Handbook, Third Edition: Volume 5, Electromagnetic Testing*. SS Udpa and PO Moore, American Society for Nondestructive Testing, Columbus, Ohio.

ASNT. 2005. *Nondestructive Testing Handbook, Third Edition: Volume 6, Acoustic Emission Testing*. RK Miller, EvK Hill and PO Moore, American Society for Nondestructive Testing, Columbus, Ohio.

Barga RS, MA Friesel and RB Melton. 1990. "Classification of Acoustic-Emission Waveforms for Nondestructive Evaluation Using Neural Networks." In *Proceedings of SPIE, Volume 1294 - Application of Artificial Neural Networks*, pp. 545-556. April 16-20, 1990, Orlando, Florida. Society of Photo-Optical Instrumentation Engineers, Bellingham, Washington.

Bates DJ, SR Doctor, PG Heasler and E Burck. 1987. *Stainless Steel Round Robin Test: Centrifugally Cast Stainless Steel Screening Phase*. NUREG/CR-4970, PNL-6266, PISC III Report No. 3, U.S. Nuclear Regulatory Commission, Washington, D.C.

Berkovits A and D Fang. 1995. "Study of Fatigue Crack Characteristics by Acoustic Emission." *Engineering Fracture Mechanics* 51(3):401-416.

Bermes C, J-Y Kim, J Qu and LJ Jacobs. 2008. "Nonlinear Lamb Waves for the Detection of Material Nonlinearity." *Mechanical Systems and Signal Processing* 22(3):638-646.

Bond LJ. 1999. "Predictive Engineering for Aging Infrastructure." In *Nondestructive Evaluation of Utilities and Pipelines III, Proceedings of SPIE*, pp. 2-13. March 4, 1999, Newport Beach, California.

Bond LJ. 2010. "Moving Beyond NDE to Proactive Management of Materials Degradation." In *Proceedings of the ASME 2010 Pressure Vessels & Piping Division / K-PVP Conference (PVP2010)*. July 18-22, 2010, Bellevue, Washington. American Society of Mechanical Engineers, New York. Paper PVP2010-26132.

Bond LJ, SR Doctor, JW Griffin, AB Hull and SN Malik. 2009a. "Damage Assessment Technologies for Prognostics and Proactive Management of Materials Degradation (PMMD)." In *Transactions 2009 ANS Annual Meeting, Advancing Nuclear Technology for a Greater Tomorrow*, pp. 215-217. June 14-18, 2009, Atlanta, Georgia. American Nuclear Society.

Bond LJ, SR Doctor, JW Griffin, AB Hull and SN Malik. 2009b. "Damage Assessment Technologies for Prognostics and Proactive Management of Materials Degradation (PMMD)." In *ANS NPIC HMIT 2009 Topical Meeting - Nuclear Plant Instrumentation, Controls, and Human Machine Interface*

*Technology*. April 5-9, 2009, Knoxville, Tennessee. American Nuclear Society, LaGrange Park, Illinois. On CD-ROM. PNNL-SA-64157.

Bond LJ, SR Doctor, JW Griffin, AB Hull and SN Malik. 2011a. "Damage Assessment Technologies for Prognostics and Proactive Management of Materials Degradation." *Nuclear Technology* 173(1):46-55.

Bond LJ, SR Doctor, JW Griffin, AB Hull and SN Malik. 2011b. "Damage Assessment Technologies for Prognostics and Proactive Management of Materials Degradation (PMMD)." *Nuclear Technology* 173:46-55.

Bond LJ, SR Doctor and TT Taylor. 2008. *Proactive Management of Materials Degradation - A Review of Principles and Programs*. PNNL-17779, Pacific Northwest National Laboratory, Richland, Washington.

Cantrell JH and WT Yost. 2001. "Nonlinear Ultrasonic Characterization of Fatigue Microstructures." *International Journal of Fatigue* 23:487-490.

Chockie AD, KA Bjorkelo, TE Fleming, WB Scott and WI Enderlin. 1991. *Maintenance Practices to Manage Aging: A Review of Several Technologies*. PNL-7823, Pacific Northwest Laboratory, Richland, Washington.

Chockie LJ. 1981. "PVRC Round Robin Ultrasonic Program, Results and Assessment of Reliability." In *Nondestructive Evaluation in the Nuclear Industry -- 1980*, pp. 361-379. February 11-13, 1980, Salt Lake City, Utah. American Society for Metals, Metals Park, Ohio.

Chockie LJ. 1985. "Section XI of the ASME Code A New Approach to Qualifying Procedures and Personnel." In *7th International Conference on NDE in the Nuclear Industry*, pp. 83-86 Grenoble, France.

Csikor FF, C Motz, D Weygand, M Zaiser and S Zapperi. 2007. "Dislocation Avalanches, Strain Bursts, and the Problem of Plastic Forming at the Micrometer Scale." *Science* 318(5848):251-254.

De S, S Palit Sagar, S Dey, A Prakash and I Chattoraj. 2010. "Quantification of Pitting in Two Tempers of 7075 Aluminium Alloy by Non-destructive Evaluation." *Corrosion Science* 52(5):1818-1823.

Diaz NJ. 2004. *The 3rd Annual Homeland Security Summit; Session on, "The Best-Laid Plans: A Case Study in Preparedness Planning": The Very Best-Laid Plans (the NRC's Defense-in Depth Philosophy)*. U.S. Nuclear Regulatory Commission. Washington, D.C. Available at http://www.nrc.gov/reading-rm/doc-collections/commission/speeches/2004/s-04-009.html.

Dobmann G. 2006. "NDE for Material Characterization of Aging Due to Thermal Embrittlement, Fatigue and Neutron Degradation." *International Journal of Materials and Product Technology* 26:122-139.

Doctor SR. 1984. "NDE Reliability Assessment." In *Non-Destructive Examination for Pressurised Components*, pp. 323-335. August 30-31, 1983, Monterey, California. Elsevier Applied Science Publishers, London.

Doctor SR. 1988. "Measurement Challenges Associated with Irradiated Reactor Components." In *Nondestructive Characterization of Materials in Aging Systems, Materials Research Society Symposium Proceedings*, pp. 163-168 Boston, Massachusetts. Materials Research Society.

Doctor SR. 2007. "Nuclear Power Plant NDE Challenges - Past, Present, and Future." In *33rd Annual Review of Quantitative Nondestructive Evaluation, Volume 26*, pp. 17-31. July 30-August 4, 2006, Portland, Oregon. American Institute of Physics, Melville, New York.

Doctor SR, P Lemaitre and S Crutzen. 1995. "Austenitic Steel Piping Testing Exercises in PISC." *Nuclear Engineering and Design* 157(1-2):231-44.

Du G, J Li, WK Wang, C Jiang and SZ Song. 2011. "Detection and Characterization of Stress-Corrosion Cracking on 304 Stainless Steel by Electrochemical Noise and Acoustic Emission Techniques." *Corrosion Science* 53:2918-2926.

Dunegan HL. 1997. "Modal Analysis of Acoustic Emission Signals." *Journal of Acoustic Emission* 15:53-61.

EPRI. 2008. *TR-105696-R11 (BWRVIP-03) Revision 11: BWR Vessel and Internals Project, Reactor Vessel and Internals Examination Guidelines* TR-1016584, Electric Power Research Institute, Palo Alto, California.

EPRI. 2011. *Materials Reliability Program: Pressurized Water Reactor Internals Inspection and Evaluation Guidelines (MRP-227-A)* TR-1022863, Electric Power Research Institute, Palo Alto, California.

Fong JT. 1986. *NDE Reliability through Round Robin Testing: Presented at the 4th National Congress on Pressure Vessels and Piping Technology, Portland, Oregon, June 19-24, 1983 and the 1986 Pressure Vessels and Piping Conference and Exhibition, Chicago, Illinois, July 20-24, 1986*. American Society of Mechanical Engineers, New York.

Gorkunov ES, YN Dragoshanskii and M Mikhovski. 2000. "Barkhausen Noise and Its Utilization in Structural Analysis of Ferromagnetic Materials (Review Article V-Effects of Volume and Surface Thermal Processing)." *Russian Journal of NDT* 36(6):389-417.

Gorman MR. 1991. "Plate Wave Acoustic Emission." *The Journal of the Acoustical Society of America* 90(1):358-364.

Gorman MR and WH Prosser. 1991. "AE Source Orientation by Plate Wave Analysis." *Journal of Acoustic Emission* 9(4):283-288.

Gorman MR and SM Ziola. 1991. "Plate Waves Produced by Transverse Matrix Cracking." *Ultrasonics* 29:245-251.

Gregor F and A Chockie. 2006. *Performance Monitoring of Systems and Active Components*. CGI Report 06:21, Chockie Group International, Inc., Seattle, Washington.

Griffith G, R Youngblood, J Busby, B Hallbert, C Barnard and K McCarthy. 2012. *Light Water Reactor Sustainability Program Integrated Program Plan*. INL/EXT-11-23452, Idaho National Laboratory, Idaho Falls, Idaho.

Hakan Gur C and I Cam. 2007. "Comparison of Magnetic Barkhausen Noise and Ultrasonic Velocity Measurements for Microstructure Evaluation of SAE 1040 and SAE 4140 Steels." *Materials Characterization* 58(5):447-454.

Harris DO and HL Dunegan. 1974. "Continuous Monitoring of Fatigue-Crack Growth by Acoustic-Emission Techniques." *Experimental Mechanics* 14(2):71-81.

Hines JW, J Garvey, J Preston and A Usynin. 2008. "Empirical Methods for Process and Equipment Prognostics (Tutorial Notes)." In *53rd Annual Reliability and Maintainability Symposium (RAMS), 2008 Proceedings*. January 28-31, 2008, Las Vegas, Nevada.

Hutton PH, MA Friesel and JF Dawson. 1993. *Continuous AE Crack Monitoring of a Dissimilar Metal Weldment at Limerick Unit 1*. NUREG/CR-5963, PNL-8844, U.S. Nuclear Regulatory Commission, Washington, D.C.

IAEA. 2003. *Assessment and Management of Ageing of Major Nuclear Power Plant Components Important to Safety*. IAEA-TECDOC-1361, International Atomic Energy Agency, Vienna, Austria.

IAEA. 2007. *Assessment and Management of Ageing of Major Nuclear Power Plant Components Important to Safety: PWR Pressure Vessel Internals, 2007 Update*. IAEA-TECDOC-1556, International Atomic Energy Agency (IAEA), Vienna, Austria.

IAEA. 2011. *Assessment and Management of Ageing of Major Nuclear Power Plant Components Important to Safety: Steam Generators, 2011 Update*. IAEA-TECDOC-1668, International Atomic Energy Agency (IAEA), Vienna, Austria.

Inman DI, CR Farrar, V Lopes and V Steffen, Eds. 2005. *Damage Prognosis*. Wiley, Chichester, West Sussex, England.

Jiles DC. 2000. "Dynamics of Domain Magnetization and the Barkhausen Effect." *Czechoslovak Journal of Physics* 50(8):893-988.

Jones RH and MA Freisel. 1992. "Acoustic Emission During Pitting and Transgranular Crack Initiation in Type 304 Stainless Steel." *Corrosion* 48(9):751-758.

Kameda J and R Ranjan. 1987. "Nondestructive Evaluation of Steels Using Acoustic and Magnetic Barkhausen Signals – I. Effect of Carbide Precipitation and Hardness." *Acta Metallurgica* 35(7):1515-1526.

Krause TW, L Clapham and DL Atherton. 1994. "Characterization of the Magnetic Easy Axis in Pipeline Steel Using Magnetic Barkhausen Noise." *Journal of Applied Physics* 75(12):7983-7988.

Krause TW, A Pattantyus and DL Atherton. 1995. "Investigation of Strain Dependent Magnetic Barkhausen Noise in Steel." *IEEE Transactions on Magnetics* 31(6):3376-3378.

Kyung-Young J. 2000. "Applications of Nonlinear Ultrasonics to the NDE of Material Degradation." *IEEE Transactions on Ultrasonics, Ferroelectrics and Frequency Control* 47(3):540-548.

Lain T. 2008. *Materials Reliability Program: Pressurized Water Reactor Issue Management Tables*. MRP-205. Rev. 1, Electric Power Research Institute, Palo Alto, California.

Lenain J-C and A Proust. 2005. "Active Corrosion Detection Using Acoustic Emission." *Materials Evaluation* 63(10):1023-1030.

Lindgren M and T Lepistö. 2001. "Effect of Prestraining on Barkhausen Noise vs. Stress Relation." *NDT&E International* 34(5):337-344.

Livingston JV, S Chattopadhyay, KR Hoopingarner, EA Pugh, WC Morgan, GD Springer and RA Pawlowski. 1995. *A Review of Information for Managing Aging in Nuclear Power Plants*. PNL-10717, Part 2 of 2, Pacific Northwest Laboratory, Richland, Washington.

Lois A and M Ruch. 2006. "Assessment of Martensite Content in Austenitic Stainless Steel Specimens by Eddy Current Testing." *Insight* 48(1):26-29.

Matlack KH, JY Kim, LJ Jacobs, J Qu and PM Singh. 2012a. "Nonlinear Rayleigh Waves to Detect Initial Damage Leading to Stress Corrosion Cracking in Carbon Steel." *AIP Conference Proceedings* 1430(1):1452-1459.

Matlack KH, JJ Wall, J-Y Kim, J Qu, LJ Jacobs and W-W Viehrig. 2012b. "Evaluation of Radiation Damage Using Nonlinear Ultrasound." *Journal of Applied Physics* 111(5):054911-1 to 054911-3.

McCloy JS, P Ramuhalli and J Henager C.H. 2012. "Use of First Order Reversal Curve Measurements to Understand Barkhausen Noise Emission in Nuclear Steel." In *Review of Progress in Quantitative Nondestructive Evaluation*. July 15-20, 2012, Denver, Colorado. American Institute of Physics, Melville, New York. To appear in Proc. QNDE 2012.

Meyer RM, JB Coble, P Ramuhalli and LJ Bond. 2011. *Advanced Instrumentation, Information, and Control System Technologies: Nondestructive Examination Technologies - FY11 Report*. PNNL-20671, Pacific Northwest National Laboratory, Richland, Washington.

Miller C. 2008. *Nondestructive Evaluation: A Review of NDE Performance Demonstrations - NDE Round Robin Report*. Report No. 1016969, Electric Power Research Institute, Palo Alto, California.

Moorthy V, S Vaidyanathan, T Jayakumar and B Raj. 1997. "Microstructural Characterization of Quenched and Tempered 0.2% Carbon Steel Using Magnetic Barkhausen Noise Analysis." *Journal of Magnetism and Magnetic Materials* 171:179-189.

Morgan WC and JV Livingston. 1995. *A Review of Information for Managing Aging in Nuclear Power Plants*. PNL-10717, Part 1 of 2, Pacific Northwest Laboratory, Richland, Washington.

Mukhopadhyay CK, T Jayakumar, B Raj and KK Ray. 2000. "Acoustic Emission--Stress Intensity Factor Relations for Tensile Deformation of Notched Specimens of AISI Type 304 Stainless Steel." *Materials Science and Engineering A* 293:137-145.

Mukhopadhyay CK, KK Ray, T Jayakumar and B Raj. 1998. "Acoustic Emission from Tensile Deformation of Unnotched and Notched Specimens of AISI Type 304 Stainless Steels." *Materials Science and Engineering A* A255(1-2):98-106.

Nichols R and N McDonald. 1987. "An Introduction to the PISC II Project--Programme for the Inspection of Steel Components." *British Journal of Nondestructive Testing* 29(4):223-227.

NRC. 2001. *Generic Aging Lessons Learned (GALL) Report*. NUREG-1801, U.S. Nuclear Regulatory Commission, Washington, D.C.

NRC. 2005a. *Generic Aging Lessons Learned (GALL) Report - Summary*. NUREG-1801, Vol. 1, Rev. 1, Office of Nuclear Reactor Regulations, U.S. Nuclear Regulatory Commission, Washington, D.C.

NRC. 2005b. *Generic Aging Lessons Learned (GALL) Report - Tabulation of Results*. NUREG-1801, Vol. 2, Rev. 1, Office of Nuclear Reactor Regulations, U.S. Nuclear Regulatory Commission, Washington, D.C.

NRC. 2010a. *Final Report - Standard Review Plan for Review of License Renewal Applications for Nuclear Power Plants*. NUREG-1800, Rev. 2, U.S. Nuclear Regulatory Commission, Washington, D.C.

NRC. 2010b. *Generic Aging Lessons Learned (GALL) Report - Final Report*. NUREG-1801, Rev. 2, Office of Nuclear Reactor Regulations, U.S. Nuclear Regulatory Commission, Washington, D.C.

NRC. 2011. *Information Digest, 2011–2012*. NUREG-1350, Vol. 23, U.S. Nuclear Regulatory Commission, Washington, D.C.

Ogi H, M Hirao and S Aoki. 2001. "Noncontact Monitoring of Surface-Wave Nonlinearity for Predicting the Remaining Life of Fatigued Steels." *Journal of Applied Physics* 90(1):438-442.

Parakka AP, J Batey, DC Jiles, M Zang and H Gupta. 1997. "Effect of Surface Mechanical Changes on Magnetic Barkhausen Emissions." *IEEE Transactions on Magnetics* 33(5):ES-09.

Pathania R. 2008. *EPRI Materials Degradation Matrix, Rev. 1*. Electric Power Research Institute, Palo Alto, California.

Perez-Benitez JA, J Capo-Sanchez, J Anglada-Rivera and LR Padovese. 2005. "A Model for the Influence of Microstructural Defects on Magnetic Barkhausen Noise in Plain Steels." *Journal of Magnetism and Magnetic Materials* 288:433-442.

Prosser WH, MA Hamstad, J Gary and A O'Gallagher. 1999. "Finite Element and Plate Theory Modeling of Acoustic Emission Waveforms." *Journal of Nondestructive Evaluation* 18(3):83-90.

Raj B, V Moorthy, T Jayakumar and KBS Rao. 2003. "Assessment of Microstructures and Mechanical Behaviour of Metallic Materials through Non-destructive Characterisation." *International Materials Reviews* 48(5):273-325.

Ramadan S, L Gaillet, C Tessier and H Idrissi. 2008. "Assessment of the Stress Corrosion Cracking in a Chloride Medium of Cables Used in Prestressed Concrete Structures by the Acoustic Emission Technique." *Measurement Science & Technology* 19(11):115702 (9 pp.).

Ramuhalli P, JW Griffin, M Dixit and LJ Bond. 2010. "Experimental Assessment of NDE Methods for Online Monitoring of Materials Degradation in Nuclear Power Plant Components." In *Transactions of the American Nuclear Society 2010 Annual Meeting*, p. 344. June 13-17, 2010, San Diego, California. American Nuclear Society, La Grange Park, Illinois.

Ramuhalli P, JW Griffin, M Dixit, JM Fricke, J Henager C.H and LJ Bond. 2011. "Nuclear Structural Materials Degradation and Remaining Life Assessment Using Integrated Diagnostics and Prognostics." Washington, D.C. Presented at 2011 ANS Winter Conference and Technology Expo, November 1, 2011. PNNL-SA-83702.

Ranjan R, O Buck and RB Thompson. 1987a. "A Study on the Effect of Dislocation on the Magnetic Properties of Nickel Using Magnetic NDE Methods." *Journal of Applied Physics* 61(8):3196-3198.

Ranjan R, DC Jiles, O Buck and RB Thompson. 1987b. "Grain Size Measurement Using Magnetic and Acoustic Barkhausen Noise." *Journal of Applied Physics* 61(8):3199-3201.

Rose JL. 1999. *Ultrasonic Waves in Solid Media*. Cambridge University Press, Cambridge, United Kingdom.

Sagar PS, N Parida, S Das, G Dobmann and DK Bhattacharya. 2005. "Magnetic Barkhausen Emission to Evaluate Fatigue Damage in a Low Carbon Structural Steel." *International Journal of Fatigue* 27(3):317-322.

Schubert F and B Schechinger. 2002. "Numerical Modeling of Acoustic Emission Sources and Wave Propagation in Concrete." *NDT.net* 7(9). Available at http://www.ndt.net/article/v07n09/07/07.htm.

Shah VK and PE MacDonald, Eds. 1993. *Aging and Life Extension of Major Light Water Reactor Components*. Elsevier Science Publishers B.V., Amsterdam.

Shaikh H, R Amirthalingam, T Anita, N Sivaibharasi, T Jaykumar, P Manohar and HS Khatak. 2007. "Evaluation of Stress Corrosion Cracking Phenomenon in an AISI Type 316LN Stainless Steel Using Acoustic Emission Technique." *Corrosion Science* 49(2):740-765.

Shaira M, N Godin, P Guy, L Vanel and J Courbon. 2008. "Evaluation of the Strain-Induced Martensitic Transformation by Acoustic Emission Monitoring in 304L Austenitic Stainless Steel: Identification of the AE Signature of the Martensitic Transformation and Power-Law Statistics." *Materials Science and Engineering A* 492:392-399.

Shintaku Y, Y Ohara, M Hashimoto, S Horinouchi and K Yamanaka. 2010. "Evaluation of Stress Corrosion Cracks in Metals by Linear and Nonlinear Ultrasound." In *20th International Congress on Acoustics (ICA 2010)*, p. 473. August 23-27, 2010, Sydney, Australia.

Shui G, J-Y Kim, J Qu, Y-S Wang and LJ Jacobs. 2008. "A New Technique for Measuring the Acoustic Nonlinearity of Materials Using Rayleigh Waves." *NDT&E International* 41(5):326-329.

Sinclair ACE, DC Connors and CL Formby. 1977. "Acoustic Emission Analysis During Fatigue Crack Growth in Steel." *Materials Science and Engineering* 28:263-273.

Sobczyk K and D Kirkner. 2001. *Stochastic Modeling of Microstructures*. Birkhauser, Boston.

Stark R. 2008. *BWR Vessel and Internals Project: Boiling Water Reactor Issue Management Tables*. BWRVIP-167NP, Rev. 1, Electric Power Research Institute, Palo Alto, California.

Stupakov O, J Pal'a, V Yurchenko, I Tomáš and J Bydžovský. 2008. "Measurement of Barkhausen Noise and Its Correlation with Magnetic Permeability." *Journal of Magnetism and Magnetic Materials* 320(3-4):204-209.

Sullivan DO, M Cotterell, DA Tanner and I Meszaros. 2004. "Characterisation of Ferritic Stainless Steel by Barkhausen Techniques." *NDT & E International* 37(6):489-496.

Sung KY, IS Kim and YK Yoon. 1997. "Characteristics of Acoustic Emission During Stress Corrosion Cracking of Inconel 600 Alloy." *Scripta Materialia* 37(8):1255-1262.

Surgeon M and M Wevers. 1999. "One Sensor Linear Location of Acoustic Emission Events Using Plate Wave Theories." *Materials Science & Engineering A (Structural Materials: Properties, Microstructure and Processing)* 265(1-2):254-261.

Wilkowski G, R Tregoning, P Scott and D Rudland. 2002. "Status of Efforts to Evaluate LOCA Frequency Estimates Using Combined PRA and PFM Approaches." In *28th MPA-Seminar*. October 2002, Universitaet Stuttgart, Germany. Materials Testing Institute.

Willetts AJ and FV Ammirato. 1987. "Objectives and Techniques for Performance Demonstration of In-Service Examination of Reactor Pressure Vessels." In *Performance and Evaluation of Light Water Reactor Pressure Vessels*, pp. 79-86. June 28-July 2, 1987, San Diego, California.

Yuyama S, T Kishi and Y Hisamatsu. 1984. "Fundamental Aspects of AE Monitoring of Corrosion Fatigue Processes in Austenitic Stainless Steel." *Journal of Materials for Energy Systems* 5(4):212-221.

Zarembo LK and VA Krasil'nikov. 1971. "Nonlinear Phenomena in the Propagation of Elastic Waves in Solids." *Soviet Physics Uspekhi* 13(6):778-797.

Pacific Northwest
NATIONAL LABORATORY

U.S. DEPARTMENT OF
ENERGY

*Proudly Operated by* Battelle *Since 1965*

902 Battelle Boulevard
P.O. Box 999
Richland, WA 99352
1-888-375-PNNL (7665)
www.pnl.gov